isvr Institute of Sound and Vibration Research

Modelling the Brain for Rotational Loading: Shear Effects and Other Complications

L. Taleb, N.S. Ferguson and C.L. Morfey

ISVR Technical Report No 276

April 1998

University of Southampton

SCIENTIFIC PUBLICATIONS BY THE ISVR

Technical Reports are published to promote timely dissemination of research results by ISVR personnel. This medium permits more detailed presentation than is usually acceptable for scientific journals. Responsibility for both the content and any opinions expressed rests entirely with the author(s).

Technical Memoranda are produced to enable the early or preliminary release of information by ISVR personnel where such release is deemed to the appropriate. Information contained in these memoranda may be incomplete, or form part of a continuing programme; this should be borne in mind when using or quoting from these documents.

Contract Reports are produced to record the results of scientific work carried out for sponsors, under contract. The ISVR treats these reports as confidential to sponsors and does not make them available for general circulation. Individual sponsors may, however, authorize subsequent release of the material.

UNIVERSITY OF SOUTHAMPTON

INSTITUTE OF SOUND AND VIBRATION RESEARCH

DYNAMICS GROUP

Modelling the Brain for Rotational Loading: Shear Effects and Other Complications

by

L. Taleb, N.S. Ferguson and C.L. Morfey

ISVR Technical Report No. 276

April 1998

Authorized for issue by
Dr M J Brennan
Group Chairman

CONTENTS

ABSTRACT

This report cover work funded by the EPSRC on the project 'Modelling Human Tolerance Limits for Transient Head Acceleration'. The second phase of the study, reported here, is concerned with modelling the brain due to rotation of the skull and this is primarily directed at lower frequency effects where the shear property of the material is important. Investigations reported here cover the effect of elastic and viscoelastic (lossy) cerebral material, the effect of the Falx protruding into the brain, the gap around the Falx and the brain filled with non viscous fluid in addition to different models of the Falx with bending or membrane stiffness. Analytical benchmark formulations are also described for the simple 2D plane strain in a cylinder produced by a half-sine rotation on the outer periphery. This allowed checking of the numerical(FE) predictions obtained using DYNA-3D. The results show the importance of the material properties, duration of loading, amplitude of loading as well as the influence of the partition and the results are shown for predicted maximum Principal strains in the models as this may well be indicative of whether damage of the brain tissue occurs.

NOTATION

The notation adopted in this report is as follows:

I: index or integer (if for fluid, s for solid, m for membrane and p for plate)
a : inner radius of the container
ρ_i: density of material i
B_i : Bulk modulus of material i
E_i: Young modulus of material i
ν_i: Poisson ratio of material i
$\Omega(t)$: angular velocity
G: Elastic shear modulus of material
$G(\omega)$: Complex shear modulus
$G_1(\omega)$: storage shear modulus
$G_2(\omega)$: loss shear modulus
G(t): relaxation function
G_0: short term shear modulus
G_∞: long term shear modulus
T: characteristic time scale of motion
c: shear wave speed $(G/\rho)^{1/2}$
Ω_{max}: magnitude of angular velocity
K: spring stiffness
$k=\omega/c$: shear wave wavenumber
d: partition penetration
h: thickness of the partition
J: gap
$\omega_{ref}= c/a$
ω_d: relaxation frequency
$\beta=\omega_d/2\pi$: viscoelastic decay constant
$S=h.E_m$: membrane stiffness
J_m: first kind Bessel function of order m
Y_m: second kind Bessel function of order m
$\Phi_i=i^{th}$ free vibration mode (elastic mat.)
u: tangential displacement
ε=shear strain
ε_{max} = maximum value reached by the Maximum principle strain

r/a: dimensionless radius
h/d: dimensionless partition thickness
j : dimensionless gap (gap/a)
$\delta=d/a$: dimensionless penetration depth
k_s: dimensionless spring stiffness K/a^3E_s
m: dimensionless membrane stiffness :hE_m/aE_s
p: dimensionless plate stiffness : h^3E_p/a^3E_s
α : dimensionless frequency ω/ω_{ref}
M: dimensionless magnitude $\Omega_{max}/\omega_{ref}$
T*: dimensionless time t/T
g : dimensionless shear modulus G_∞/G_0
b : dimensionless relaxation frequency β/ω_{ref}
ka: Helmholtz number

1.0 INTRODUCTION

Investigators into head injury research are agreed that the head injury mechanism related to the Diffuse Axonal Injury (DAI) is due to a rotational acceleration of the head, normally as the result of some specified impact. This rotation may cause considerable shearing strains and distortions in the brain, particularly in regions where further rotation is prevented by bony protrusions inside the cranium. Holbourn (1943), in one of the earliest applications of photoelasticity to experimental biomechanics, observed the shear stress distribution in a wax-skull and gelatine-brain model subjected to rotational acceleration. Holbourn related the degree of strain, indicated by the model, to the amount of stretch of the neural and vascular fibres in the region, and thus to injury severity. This was the first study to draw attention to the relatively strong influence of rotational acceleration over translational acceleration in causing brain damage. Further elucidation on the subject was provided by Gennarelli et al. (1972), who reported that the average number of concussions recorded was higher when squirrel monkeys were subjected to rotational acceleration than to translational acceleration. Margulies et al. (1990) performed experiments on a physical model to simulate brain injuries. They noted that when the head model was subjected to tangential acceleration, the regions of the brain where shear strains were largest corresponded to locations of diffuse axonal injury from clinical observation. It was decided that shear strain could be used as an index for angular acceleration induced tissue injury. It was then proposed that the angular acceleration limit for DAI in the human brain was 16000 rads/s^2.
Galbraith et al. (1993) investigated the response of the squid giant axon to strain. Ability to conduct action potentials was monitored with respect to stretch injury. It was found that 12% elongation performed within 14 ms suppressed nerve activity for 3 minutes. As the loading rate increased, the injury response became more pronounced and longer lasting. After 20% elongation, 90% of the nerve resting potential was eventually regained, but after more than 20 % elongation, the axon would never fully recover. Elongation of 25 % resulted in structural failure. Similar results were reported by Thibault et al. (1992).

In recent years both numerical and analytical models have been used to study the dynamic shear response of the brain (Firoozbaksh and DeSilva (1975); Liu et al. (1975); Ljung (1975, 1980), Lee et al. (1987), Ueno and Melvin 1990, Chu and Lee (1991); Trosseille et al. (1992). Most of these studies concluded that when the head is subjected to rotational loading, large shear stresses are developed near the vertex of the brain where the parasagittal bridging vein is located. This may lead to rupture of the vein and consequently, subdural haematoma reported by Chu and Lee, 1991. In an earlier study, Lee et al. (1987) reported that as the brain incompressibility increases, the influence of rotational acceleration on the deformation of the parasagittal bridging vein becomes stronger than that for translational acceleration.
From numerical studies Trosseille et al. (1992) concluded that if a blow is applied to the head along the sagittal plane, in addition to the parietal region, relatively large shear strains also develop at the cranio-spinal junction (brain stem). Similarly Ueno and Melvin (1990) concluded that when the head is subjected to purely rotational acceleration in the

sagittal plane, large shear stresses were computed in the parietal and brain stem region. In a more recent three dimensional Finite Element study, Kumaresan and Radhakrishnan (1995) in which a head neck model was used, it was observed that the largest shear strain developed in the region above the foramen magnum.

Previous studies have shown the influence of the partitioning membrane on the distribution of pressure in the brain and on it's modal behaviour (Trosseille et al. 1992, Kumaresan and Radhakrishnan 1995, Ruan et al 1991). Bandak and Eppinger 1994, focused their work on the effect of a combined rotational and translational acceleration loading on the evolution of strain in the brain. To our knowledge, no previous explicit study discusses the effect of the membrane on the dynamic shear response of the brain.

In studying the shear response of the brain, two semi-analytical solutions of the forced response of the brain are described in this report. No exact analytical solution is available for the general forced response and only numerical results can be obtained. The first solution, valid for the viscoelastic material models and can be applied for elastic models with non-zero damping , uses the Fast Fourier Transform technique. The second procedure is based on a modal decomposition of the response in the time domain and is applicable to elastic models with or without damping. The latter technique uses the free vibration mode shapes as a basis for evaluating the response. Typically the problems being considered are for rotations of short duration (i.e. transient or non-steady conditions) and one is interested not only in the magnitude of the response but when the maxima occur. For long duration events the problem becomes quasi-static and there are usually small dynamic contributions involved . These solutions will serve as a reference to compare and validate the parallel investigations using a Finite Element (FE) model and to evaluate how well the FE code reproduces the physical behaviour.

A two dimensional FE plane strain model consisting of a simple rigid cylinder filled with a material, and partitioning membrane, subjected to a prescribed rotational velocity has been developed. For expediency, the container will be referred to the skull and the contents to the cerebral matter. Linear elastic as well as linear viscoelastic material properties were assigned to the brain tissue. The viscoelastic properties used here were to investigate the influence of a time-dependent constitutive material model on the head's response, rather than to make an attempt to accurately describe its material behaviour.

A qualitative assessment of the effect of the partitioning membrane has been obtained by studying different container-partition attachment and different material formulation of the partition as:

(i) rigid partition attached to the skull,

(ii) membrane description of the partition(tensile effects)

(iii) plate formulation(allowing both tensile and bending contributions).

A sliding interface is imposed at the Brain-Skull boundary. Additional complexities were gradually introduced by including a cerebrospinal fluid layer between the partition and the brain, as well as between the skull and the brain. The effect of the depth of penetration of the partition, as well as the thickness of the layer of fluid between the partition and the brain, namely the gaps, on the rotational response of the material have been also studied.

The computations were performed using an explicit commercial code (DYNA-3D) and the various material models were the standard formulations available in the software. The numerical models used for validation purposes were considered only for models without partitions as the model with partitions requires a model with both shear and normal stresses.

2.0 INVESTIGATION OF MATERIAL MODELS

2.1 Experimentation on Brain Tissue

In the analysis of the viscoelastic properties of the brain tissue, the most commonly employed stress histories or strain histories are step function stress histories (creep), step function strain histories (stress, relaxation), ramp function strain histories, and sinusoidal stress or strain histories. Many attempts for measuring these properties are reported in the literature (Fallenstein and Hulce 1969, Galford and McElhaney 1970, Hirakawa et al. 1981). Generally, the characterisation of brain tissues is given in term of a complex shear modulus [$G(\omega) = G_1(\omega)+jG_2(\omega)$]. Experimental values of the shear modulus lie in the range 1 to 82 kPa (see table 1). Hicling and Wener (1973), in discussing a mathematical model for head impact problems, indicated that the value of the complex shear modulus is required for the frequency range of 0 to 2200 Hz. It is evident, therefore, that further experimentation on human brain tissue is needed at the higher frequencies.

Table 1: Literature review of rheological properties of human brain tissue

Author	G_1 [kPa]	G_2 [kPa]	Loss tangent	comments
Fallenstein 1969	6.9-1.1	3.5 - 6	0.4 - 0.55	9-10 Hz at 37 °C
Galford 1970	66.74	26.2		Compression Bulk = 2E+09 Pa; 10-40 Hz
Shuck 1972	8.350 - 33	3.45 - 81.4		5 - 350 Hz
Hirakawa 1981	White matter: 6.5-12 Grey matter: 1.5-2.5	White matter: 4 - 12 Grey matter: 2.4-5.4		temp = 36 °c 3 - 35 Hz

The most interesting data given for G_1 and G_2 ,for human brain tissue, were reported by Shuck and Advani (1972). They performed a torsional response experiment on human brain tissue in the frequency range from 5 - 350 Hz. The tabulated complex shear modulus results can be expressed in terms of the shear relaxation function G(t) by:

$$G_1(\omega) + jG_2(\omega) = \int_{-\infty}^{\infty} G(t)e^{-j\omega t}dt\,,$$

with

$G(t) = G_\infty + G_1 e^{-\beta_1 t}+...+G_n e^{-\beta_n t}$ can be used to determine the shear modulus constants G_∞, G_1, ..., G_n and relaxation constants β_1,.., β_n.

Different rheological models (see section 2.3) have been used to describe the shear response of the brain. For a specific model, the relaxation function constants were obtained by fitting the complex shear modulus described by the model to experimental data. The values used in the literature for these three viscoelastic material components are cover a wide range. Figure 2.1 shows how these values differ.

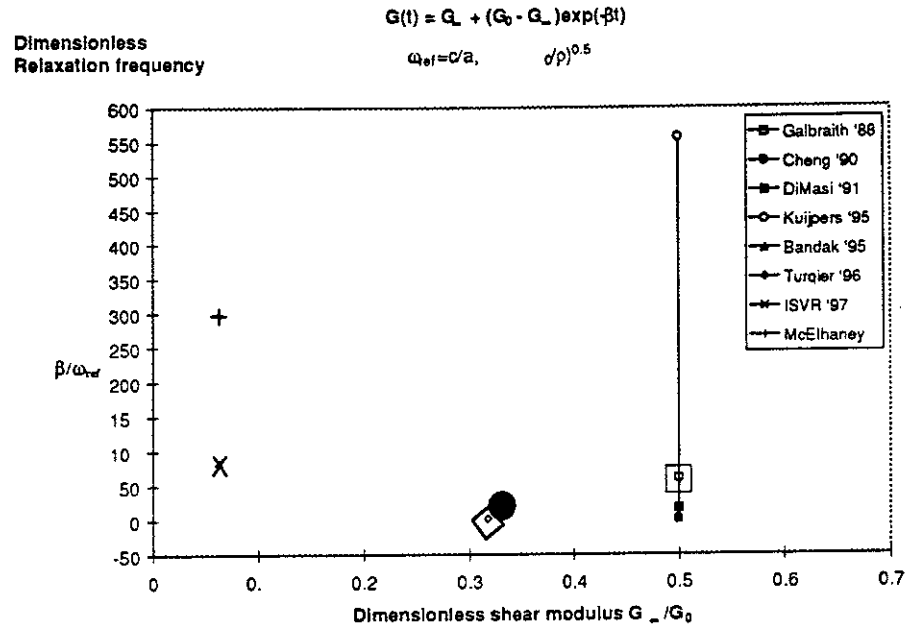

Figure 2.1 Published values of the viscoelastic parameters for brain tissue

Previously published experimental data by Shuck and Advani (1972) are limited to a low frequency range(10-350 Hz). It is not possible to have a very good fit in this range of frequency for the Boltzmann model (see section 2.2.3) used in this work, because the loss modulus is very sensitive to frequency. However, it is believed that the complex shear modulus at high frequency is more representative to the shear modulus of brain tissue. Hence the fitted data are based on the range over 80 Hz. The values which give a good fit were taken as G_0 = 320 kPa, G_∞=20 kPa and β = 1360 s^{-1}. In addition the bulk modulus used for the nearly incompressible brain material is 2.083e9 Pa. Figure 2.2 illustrates the experimental complex shear modulus components ($G_1(\omega)$ and $G_2(\omega)$) and the fitted Boltzmann model components.

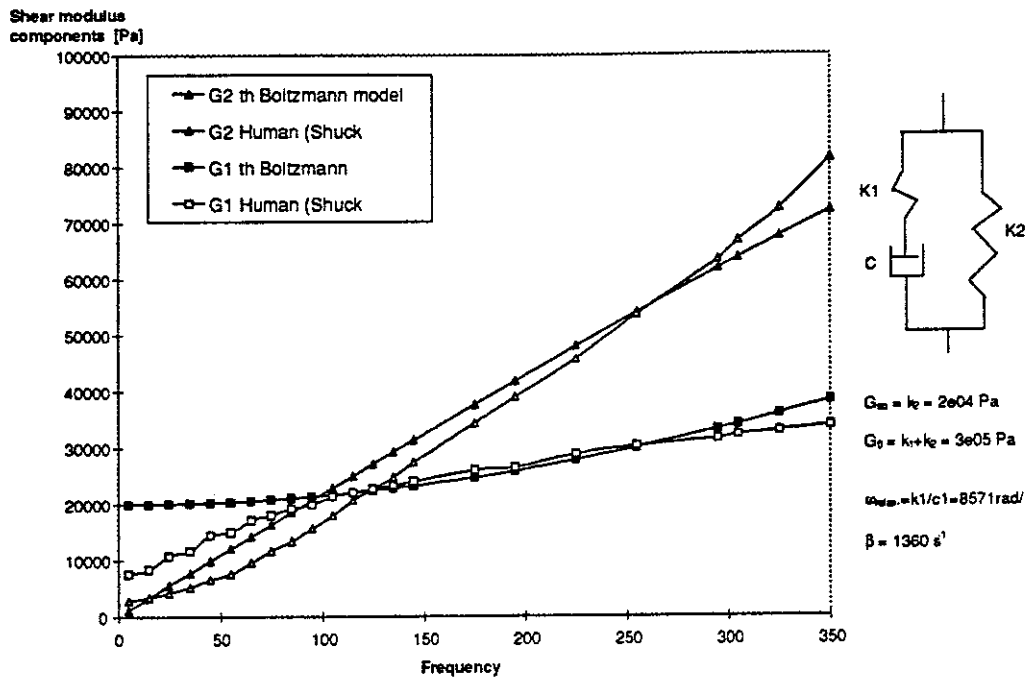

Figure 2.2 Standard model matched to previously published human brain tissue shear modulus data (Shuck and Advani. 1972).

2.2. Modelling Brain Tissue

In all models presented the different biological tissues were assumed to be homogeneous and isotropic. The main difficulty in the material modelling is at the constitutive equation level of the brain material. As a first approximation, nearly all models suppose a linear elastic solid and use small-deformation theory. More recently explicit FE codes use large-deformation theory. The elastic linear material properties frequently used are the Young's modulus of Elasticity, E, and Poisson's ratio, ν. The Bulk modulus, B, and shear modulus,G, are deduced using the following relationships:

$$G = \frac{E}{2(1+\nu)} \qquad \text{and} \qquad B = \frac{E}{3(1-2\nu)}$$

This is despite the well-known fact that the head accelerations during a typical automobile crash can lead to irreversible mechanical changes and even rupture surfaces in the brain tissue.

Modern finite element codes allow for the introduction of linear viscoelastic constitutive equations. The simplest material behaviour is characterised by a time dependant shear modulus with a single non-zero relaxation constant as follows:

$$G(t) = G_\infty + (G_0 - G_\infty)e^{-\beta t}$$

where G_0, G_∞ and β correspond to the instantaneous and long term shear moduli in time and the relaxation constant respectively(see following section).

2.3. Constitutive Viscoelastic Models

2.3.1 Maxwell and Kelvin-Voigt Models

The Maxwell and Kelvin-Voigt viscoelastic models are shown in figure 2.3.1 below.

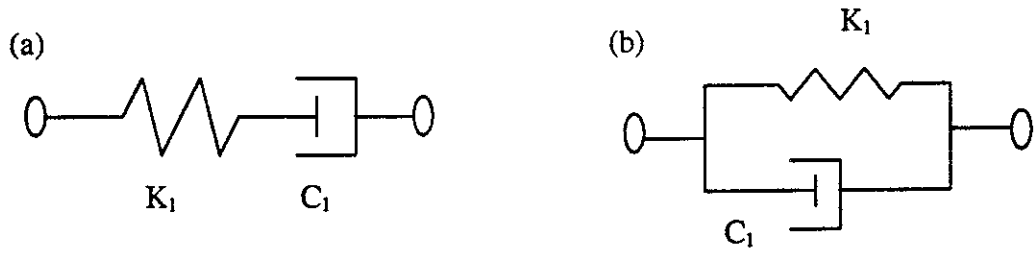

Figure 2.3.1. Schematic of (a) Maxwell Model and (b) Kelvin-Voigt Model

For the Maxwell model

$$\frac{\sigma}{C_1}+\frac{\dot{\sigma}}{K_1}=\dot{\varepsilon} \qquad \Rightarrow \qquad \frac{\bar{\sigma}}{\bar{\varepsilon}}=G(\omega)=j\omega[\frac{1}{C_1}+j\frac{\omega}{K_1}]^{-1}$$

where $\bar{\sigma}$, $\bar{\varepsilon}$ are the frequency spectrum of the stress and strain, and $G(\omega)$ is the overall complex modulus.

For the Kelvin-Voigt model,

$$\sigma = K_1\varepsilon + C_1\dot{\varepsilon} \qquad \Rightarrow \qquad G(\omega)=\frac{\bar{\sigma}}{\bar{\varepsilon}}=K_1+j\omega C_1$$

In the time domain, the stress-strain relaxation models are described in terms of the convolution integral of the relaxation function and the strain or strain rate terms. For numerical purposes the commonly used formulation is in terms of strain rate:

$$\sigma(t)=\int_0^t G(t-\tau)\frac{\partial\varepsilon(\tau)}{\partial\tau}d\tau$$

The corresponding relaxation functions in time are:

(a) Maxwell model:

$G(t)=K_1e^{-\frac{K_1}{C_1}t}$ (i.e. relaxation only)

(b) Voigt model

$G(t)=K_1+C_1\delta(t)$ (i.e. elastic with no relaxation of the real modulus)

2.3.2. Maxwell - Kelvin Voigt Model-Standard Model

The constitutive relationship for this system

(see figure 2.3.2) is:

$$K_2C_1\dot{\varepsilon} + K_1K_2\varepsilon = (K_1 + K_2)\sigma + C_1\dot{\sigma}$$

$$(K_1K_2 + j\omega K_2C_1)\varepsilon = (K_1 + K_2 + j\omega C_1)\sigma$$

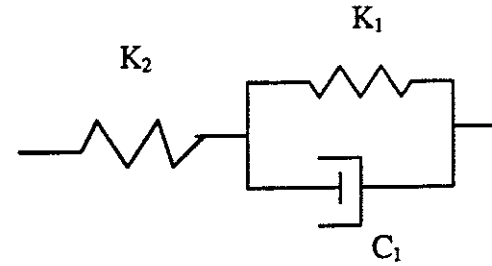

Figure 2.3.2. Schematic of Maxwell Kelvin-Voigt Model (Standard Model)

The complex shear modulus is:

$$G(\omega) = \frac{K_1K_2 + j\omega K_2C_1}{(K_1 + K_2) + j\omega C_1} = K_2 - \frac{\frac{K_2^2}{C_1}}{\frac{K_1 + K_2}{C_1} + j\omega}$$

This model has relaxation in the real modulus and the complex modulus has a peak value at $\omega = \omega_d = \frac{K_1 + K_2}{C_2}$, the relaxation frequency.

In the frequency domain one can write

$$G_0(\omega) = G_{\omega\to 0} = \frac{K_1K_2}{K_1 + K_2},\ G_\infty(\omega) = G_{\omega\to\infty} = K_2 \text{ and } \omega_d = \frac{K_1 + K_2}{C_1}$$

In the time domain, the relaxation function is defined by:

$$G(t) = G_\infty + (G_0 - G_\infty)e^{-\beta t} \text{ with } G_0 = K_2\ ,\ G_\infty = \frac{K_1K_2}{K_1 + K_2} \text{ and } \beta = \frac{1}{2\pi}\frac{K_1 + K_2}{C_1} \text{ (in Hz)}$$

where G_0, G_∞ and β correspond to the short term shear modulus, the long term shear modulus and the viscoelastic relaxation constant respectively.

2.3.3. Boltzmann Model -Three Parameter Maxwell Model

For a three parameter Maxwell model known as Boltzmann model (see figure 2.3.3 below), the complex shear modulus is defined in the frequency domain by,

$$G(\omega) = K_2 + \frac{j\omega K_1C_1}{K_1 + j\omega C_1}$$

By substituting

$$G_0(\omega) = G_{\omega\to 0}(\omega) = K_2\ ,\ G_\infty(\omega) = G_{\omega\to\infty}(\omega) = K_1 + K_2\ ,\ \text{and } \omega_d = \frac{K_1}{C_1}\ ,$$

one can write,

$$G(\omega) = G_0(\omega) + \frac{\big(G_\infty(\omega) - G_0(\omega)\big)j\omega}{\omega_d + j\omega},$$

The relaxation function is defined as ,

$$G(t) = G_\infty + (G_0 - G_\infty)e^{-\beta t} \quad \text{with} \quad G_0 = K_1 + K_2 \ , \ G_\infty = K_2 \text{ and } \beta = \frac{1}{2\pi}\frac{K_1}{C_1} \text{ (in Hz).}$$

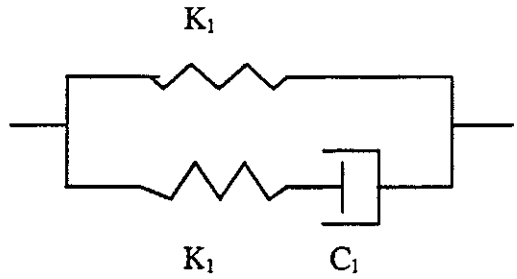

Figure 2.3.3. Schematic of Three Parameters Maxwell Model (Boltzmann Model)

3. BENCHMARK TEST

This section focuses on the response of elastic and viscoelastic materials contained within a rigid cylinder that undergoes axisymmetric rotation, $\Omega(t) = \Omega_{max} \sin \omega_1 t$, as shown in the figure 3.1, below.

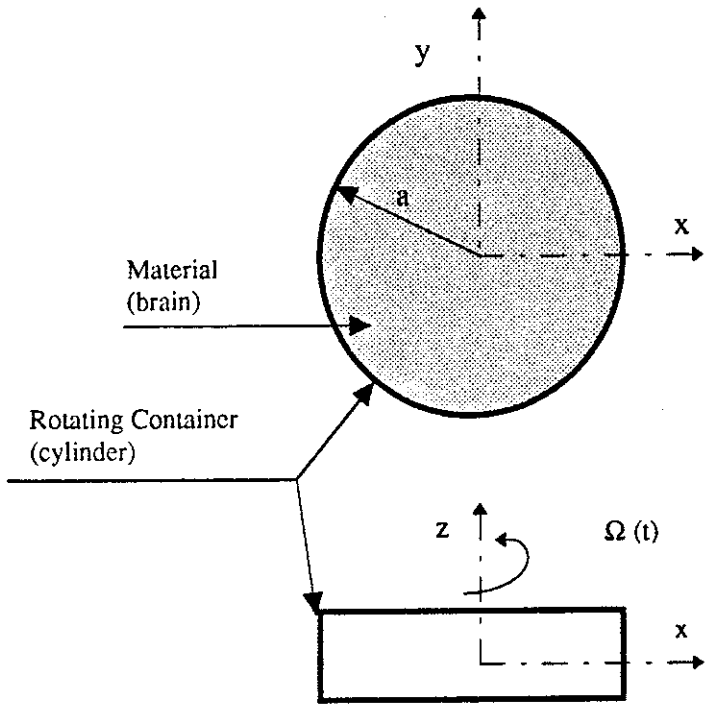

Figure 3.1: Rotating container filled with elastic material

3.1. Analysis for Harmonic Time Dependent Boundary Conditions

The analysis is based on the following assumptions:

(1) only plane motion occurs, i.e. the cylinder of outer radius a, can be considered as infinitely long and deformation does not occur in the axial (z) direction,

(2) there is no slip at the interface of the material and the container (i.e. the outer radius of the material r = a, rotates with the container),

(3) The material is incompressible,

(4) axisymmetric rotation causes displacement ($u = u_\theta$) to only occur in the circumferential (θ) direction and no displacement in the radial r direction.

Assumption (3) can probably be relaxed as axisymmetric rotation would not, for this simple cylindrical geometry, be expected to cause compressible wave/effects to be generated. The displacement u is then a function of radius r and time t. The non-zero shear strain is given by $\varepsilon = \varepsilon_{r\theta}$, where

$$\varepsilon = \frac{1}{2}\left(\frac{\partial u}{\partial r} - \frac{u}{r}\right) \tag{3.1.1}$$

For elastic material the constitutive relationship is

$$\sigma = G\varepsilon \tag{3.1.2}$$

Previous work of Margulies and Thiobault 1989 considered the response of the material due to a harmonic component of a fourier series with specified initial condition. The present solution describes the response of the material to any frequency harmonic rotation. The boundary conditions used here are:

$$\begin{cases} u(r=0,t)=0 \\ and \\ \dot{u}(r=a,t)=\dot{U}_0 e^{j\omega t} \end{cases} \qquad \begin{cases} u(r=0,t)=0 \\ and \\ u(r=a,t)=\dfrac{\dot{U}_0}{j\omega} e^{j\omega t} \end{cases} \tag{3.1.3}$$

The equation of motion for the displacement of the elastic material in the θ direction is given by

$$\frac{\partial^2 u}{\partial t^2} = c^2\left(\frac{\partial^2 u}{\partial r^2} + \frac{1}{r}\frac{\partial u}{\partial r} - \frac{u}{r^2}\right) \tag{3.1.4}$$

where c is the shear wave speed.

The solution of equation (3.1.4), similar in form to the wave equation in cylindrical coordinates (Skudrzyk 1971), does not require the introduction of potentials. A separable form of the solution is used,

$$u(r,t) = u(r)T(t) \tag{3.1.5}$$

Substituting into equation (3.1.4) gives

$$u\frac{d^2T}{dt^2} = c^2\left(u'' + \frac{u'}{r} - \frac{u}{r^2}\right)T \tag{3.1.6}$$

or

$$\frac{\ddot{T}}{T} = \frac{c^2}{u}\left(u'' + \frac{u'}{r} - \frac{u}{r^2}\right) \tag{3.1.7}$$

The left-hand side is only a function of time t, and the right-hand side is only a function of r. Hence both sides must be equal to an arbitrary constant, $-\lambda^2$, say.

$$\ddot{T} + \lambda^2 T = 0 \tag{3.1.8}$$

has solutions $$T = Ae^{j\lambda t} + Be^{-j\lambda t} \tag{3.1.9}$$

with arbitrary constants A and B.

The equation for u is

$$\frac{d^2u}{dr^2} + \frac{1}{r}\frac{du}{dr} - \frac{1}{r^2}u + \frac{\lambda^2}{c^2}u = 0$$

i.e. $$\frac{d^2u}{dr^2} + \frac{1}{r}\frac{du}{dr} + (\frac{\lambda^2}{c^2} - \frac{1}{r^2})u = 0 \tag{3.1.10}$$

Equation (3.1.10) has a similar form to the general Bessel equation that occurs in problems such as sound propagation in circular tubes (Skudrzyk 1971). The solution of this equation is:

$$u(r) = CJ_1(\frac{\lambda}{c}r) + DY_1(\frac{\lambda}{c}r) \tag{3.1.11}$$

where J_1 and Y_1 are the Bessel functions of the first and second kind of order one.

By putting $\lambda = \omega$ and $k = \frac{\omega}{c}$, equivalent to the shear wave wavenumber, the solution for the steady-state displacement of the elastic material is then given as

$$u(r,t) = (Ae^{j\omega t} + Be^{-j\omega t})(CJ_1(kr) + DY_1(kr)) \tag{3.1.12}$$

Using the boundary conditions defined by equation (3.1.3),

$$u(r = a, t) = \frac{\dot{U}_0}{j\omega}e^{j\omega t} \qquad B = 0$$

rotation $$u(0,t) = 0 \quad \Rightarrow \quad CJ_1(0) + DY_1(0) = 0$$

$$u(a,t) = \frac{\dot{U}_0}{j\omega}e^{j\omega t} \quad \Rightarrow \quad A(CJ_1(ka) + DY_1(ka)) = \frac{\dot{U}_0}{j\omega}$$

Equation (3.1.13-3.1.15) respectively.

As $J_1(0) = 0$ and $Y_1(0) = -\infty$, the finite solution requires

$$\begin{cases} D = 0 \\ AC = \dfrac{\dot{U}_0}{j\omega J_1(ka)} \end{cases}$$

The final solution is: $u(r,t) = \dfrac{\dot{U}_0}{j\omega}\dfrac{J_1(kr)}{J_1(ka)}e^{j\omega t} \Rightarrow \dot{u}(r,t) = \dot{U}_0\dfrac{J_1(kr)}{J_1(ka)}e^{j\omega t}$ (3.1.16)

Equation (3.1.16) has singularities at the zeros of $J_1(ka)$, corresponding to the natural frequencies of the elastic material in shear, i.e. ka = 3.83, 7.02, 10.17, etc.

Likewise the transfer function $H(\omega)$, equal to the displacement of the material divided by the rotational velocity of the boundary at frequency ω, is given as

$$H(\omega) = \frac{u(r,t)}{\dot{U}_0 e^{j\omega t}} = \frac{1}{j\omega}\frac{J_1(kr)}{J_1(ka)} = \frac{1}{j\omega}\frac{J_1\left(ka\dfrac{r}{a}\right)}{J_1(ka)} \tag{3.1.17}$$

h(t), the impulse response function, could be obtained by inverse Fourier transform of $H(\omega)$. No analytical result is available and only numerical results can be produced using Fast Fourier Transform techniques.

The transfer function for the strain $\varepsilon(\omega)$, due to unit velocity, can similarly be obtained by substituting for the displacement u(r,t) into equation (3.1.1) and using the relationships for the derivatives of the Bessel functions (Kreyszig 1992).

$$\varepsilon(\omega) = \frac{1}{j\omega}\frac{1}{2aJ_1(ka)}\left[(ka)J_0(ka\frac{r}{a}) - 2\frac{J_1(ka\frac{r}{a})}{\frac{r}{a}}\right] = -\frac{1}{j\omega}\frac{(ka)J_2\left(ka\dfrac{r}{a}\right)}{2aJ_1(ka)} \tag{3.1.18}$$

In equations (3.1.17) and (3.1.18) it has been possible to introduce non-dimensional parameters using the term "ka", known as the Helmholtz number, and r/a the ratio of the radial position to the outer radius.

Numerically, the impulse response function for the displacement and the strain can be more easily obtained for viscoelastic or damped materials as the transfer functions are finite at all frequencies. For the undamped elastic material consider the point on outer radius, r = a. Then $H(\omega)=1/j\omega$ and the impulse response function, for the velocity on the periphery, is the Dirac delta function as expected.

One could, in general, also use a modal approach to obtain the solution for finite duration inputs by expressing the solution in terms of the corresponding modes (eigenfunctions) with the natural frequencies (eigenvalues) (Stephenson 1974). This is described in the following section for a particular imposed boundary condition for the elastic case.

3.2. A modal solution for harmonic imposed boundary conditions and for a half sine input.

3.2.1. General solution

The previous analysis of the steady state response of the elastic material can be extended, using a modal expansion (Stephenson 1974), to include free vibration effects that are important for lightly damped systems or for predicting the response of the system to short duration (transient) or non-steady conditions. As an example of the approach consider the following boundary conditions on the boundary r = R = a,

$$u(a,t) = \begin{cases} A\sin\omega t & 0 \le t < \dfrac{\pi}{\omega} \\ & \Rightarrow \\ 0 & \dfrac{\pi}{\omega} < t \end{cases} \qquad (3.2.1)$$

This is known as a half sine pulse and is used to investigate the maximum response as a function of ω(or usually ω/ω_n for a system with natural frequency ω_n). By linear superposition the boundary condition can also be written as,

$$u(a,t) = \begin{cases} A\sin\omega t & 0 \le t < \dfrac{\pi}{\omega} \qquad (3.2.2) \\ & \Rightarrow \\ A\sin\omega t + A\sin\omega(t-\pi/\omega) & \dfrac{\pi}{\omega} < t \qquad (3.2.3) \end{cases}$$

And the problem reduces to the solution of the elastic material due to a harmonic input (for $t < \pi/\omega$) and the summation (for $t > \pi/\omega$) of a delayed version of the solution with the original solution.

for $t < \pi/\omega$ consider the solution for the imposed boundary conditions:

$$u(a,t) = A\sin\omega t \qquad t > 0$$

$$u(r,0) = 0 \qquad (3.2.4)$$

$$\dot{u}(r,0) = 0 \qquad (3.2.5)$$

The last two conditions are due to the material being initially at rest. The displacement, u, of the material is given by the steady-state solution (see previous section) and the free vibration in the modes $\Phi_i(r)$ of the elastic material. The total solution consists of a linear combination of the modes (eigenfunctions) with an infinite set of coefficients (A_i and B_i) in conjonction with the steady-state solution. The coefficients are chosen such that the boundary conditions (equations 3.2.4) and (3.2.5) are satisfied (Stephenson 1974), i.e.

$$u(r,t) = A\sin\omega t \frac{J_1\left(ka\dfrac{r}{a}\right)}{J_1(ka)} + \sum_{i=1}^{\infty}(A_i\cos\omega_i t + B_i\sin\omega_i t)\Phi_i(r) \qquad (3.2.6)$$

ω_i is the corresponding natural frequency for the Φ_i mode.

The modes Φ_i could be obtained for various boundary conditions (on r = 0 and r = a) but if one chooses the modes corresponding to zero displacement at the centre (r = 0) and the outer periphery (r = a) the solution, as given by equation (3.2.6), would then automatically satisfy the boundary condition on r = a (equation (3.2.4)).

The modes corresponding to the specified boundary conditions are,
$\Phi_i(r) = J_1(k_i r)$
where k_i are the values such that $J_1(k_i a)=0$, i.e. $k_i a$ = 3.83, 7.02,..., etc. The undamped natural frequencies, ω_i are given by $(k_i c)$ with $c = \sqrt{\frac{G}{\rho}}$.

Substituting the series solution, equation (2.6), into equations (2.4) and (2.5) one has

$$\sum_{i=1}^{\infty} A_i \Phi_i(r) = 0 \tag{3.2.7}$$

and

$$\omega A \frac{J_1(kr)}{J_1(ka)} + \sum_{i=1}^{\infty} B_i \omega_i \Phi_i(r) = 0 \tag{3.2.8}$$

It can be shown that the modes of the system are orthogonal (Stephenson 1974 p.67-73 for a similar boundary value problem, and Gradshteyn and Ryzhik 1983, expression 6.52), i.e.

$$\int_0^a r J_1(\lambda_i r) J_1(\lambda_j r) dr = 0 \qquad \text{i}\neq\text{j and } J_1(\lambda_i a) = J_1(\lambda_j a) = 0 \tag{3.2.9}$$

$$\int_0^a r J_1{}^2(\lambda_i r) dr = \frac{a^2}{2}\left[J_1{}'(\lambda_i a)^2 + (1 - \frac{1}{\lambda_i{}^2 a^2}) J_1{}^2(\lambda_i a) \right]$$

$$\equiv \frac{a^2}{2} J_2{}^2(\lambda_i a) \tag{3.2.10}$$

Hence using the orthogonality property one can show, using equation (3.2.7), that A_i=0 for all i. The coefficients B_i can also be obtained.

$$B_i = -\frac{\omega A \int_0^a \frac{r J_1(kr) J_1(k_i r)}{J_1(ka)}}{\omega_i \int_0^a r J_1{}^2(k_i r) dr}$$ By putting $\psi = ka$ and $\gamma = k_i a$, we can define B_i as,

$$B_i = \frac{-2\psi A}{\gamma} \frac{\int_0^1 z J_1(\psi z) J_1(\gamma z) dz}{J_1(\psi) J_2{}^2(\gamma)} \tag{3.2.11}$$

NB. Assumption that ω, the excitation frequency, is not equal to any ω_i, natural frequency, otherwise $J_1(ka)=0$ (see later for the result when $\omega=\omega_i$).

The integral in the numerator of equation (3.2.11) $\int_0^a rJ_1(kr)J_1(k_i r)dr$, is a particular finite Hankel transform . Margulies and Thibault 1989, used it to transform the original equation of motion. Herein it is used to obtain the modal contributions.
The final solution is,

$$u(r,t)=A\sin\omega t\frac{J_1\left(ka\frac{r}{a}\right)}{J_1(ka)}+\sum_{i=1}^{\infty}\frac{-2\psi A}{\gamma}\frac{\int_0^1 zJ_1(\psi z)J_1(\gamma z)dz}{J_1(\psi)J_2{}^2(\gamma)}\sin\omega_i tJ_1(k_i r) \tag{3.2.12}$$

3.2.2. *Case* $\omega=\omega_i$

The special case is when $\omega=\omega_i$, i.e. frequency of applied harmonic boundary condition is at the i^{th} natural frequency of the material (equivalent to $k=k_i$).

The coefficient $B_i=0$ for $i\neq j$, due to the orthogonality relationship equation (3.2.9), and,

$$B_j=\lim_{\omega\to\omega_j}\frac{-\omega A}{\omega_j}\frac{1}{J_1(ka)} \tag{3.2.13}$$

The solution then simplifies to

$$u(r,t)=\lim_{\omega\to\omega_j}\left[A\sin\omega t\frac{J_1(kr)}{J_1(ka)}-\frac{\omega A}{\omega_j}\frac{\sin\omega_j tJ_1(k_j r)}{J_1(ka)}\right] \tag{3.2.14}$$

First inspection would indicate that the response becomes infinite, as $J_1(k_j a)=0$, but taking the limit (using l'Hôpital's rule):

$$u(r,t)=\frac{Ac}{a}\frac{1}{J_1'(k_j a)}\left[J_1(k_j r)t\cos\omega_j t+\sin\omega_j t\left(J_1'(k_j r)\frac{r}{c}-\frac{J_1(k_j r)}{\omega_j}\right)\right]$$

As $J_1(z)=J_0(z)-\frac{J_1(z)}{z}$ (see Kreyszig 1992) and $J_1(k_j a)=0$, then,

$$u(r,t)=\frac{Ac}{a}\frac{1}{J_0(k_j a)}\left[J_1(k_j r)t\cos\omega_j t+\sin\omega_j t\left(J_1'(k_j r)\frac{r}{c}-\frac{J_1(k_j r)}{\omega_j}\right)\right]$$

$$u(r,t)=\frac{Ac}{a}\frac{1}{J_0(k_j a)}\left[J_1(k_j r)t\cos\omega_j t+\frac{\sin\omega_j t}{c}\left(rJ_1'(k_j r)-\frac{J_1(k_j r)}{k_j}\right)\right] \qquad (3.2.15)$$

NB. Equation (3.2.15) shows that the response on the boundary is finite, and equal to $A\sin\omega_j t$, but at interior points the response is increasing due to the "$t\cos\omega_j t$" term. The analytical solution for the response can now be obtained for any harmonic component, or half sine impulse, using equations (3.2.3) and (3.2.6) with relevant coefficients B_j.

3.2.3. Case Study: Applied Half-Sine Velocity Input to 2D Cylindrical Sample

Let the outer periphery attached to the elastic or viscoelastic material, be subjected to a velocity that is described by a half-sine pulse. i.e.

$$\dot{u}(a,t)=\begin{cases}A\sin\omega t & 0\le t<\dfrac{\pi}{\omega} \qquad (3.2.3.1)\\ 0 & \dfrac{\pi}{\omega}<t \qquad (3.2.3.2)\end{cases}$$

The corresponding displacement on the periphery is

$$u(a,t)=\begin{cases}\dfrac{A}{\omega}(1-\cos\omega t) & 0\le t<\dfrac{\pi}{\omega} \qquad (3.2.3.3)\\ \dfrac{2A}{\omega} & \dfrac{\pi}{\omega}<t \qquad (3.2.3.4)\end{cases}$$

The factor A/ω ensures that $u(a,0)=0$. i.e. the motion has zero initial velocity and displacement.
The response of the material can be described by the superposition of two displacement inputs, namely

$$u(a,t)=\frac{A}{\omega}(1-\cos\omega t) \qquad 0\le t \qquad (3.2.3.5)$$

and

$$u(a,t)=\frac{A}{\omega}(1-\cos\omega t)-\frac{A}{\omega}(1+\cos\omega(t-T) \qquad T=\frac{\pi}{\omega}<t \qquad (3.2.3.6)$$

The solution is based on the steady state solution of the equation of motion of the material with the boundary conditions described by (3.2.3.3) and (3.2.3.4) or correspondingly by (3.2.3.5) and (3.2.3.6) with the transient solution given in terms of the free vibration modes of the cylinder, namely $u(r,t)=J_1(k_i r)e^{j\omega_i t}$, where "$k_i a$" takes certain values for a boundary free of displacement.

In particular for elastic material, considering equation (3.2.3.5), the steady state solution when the displacement on the periphery given by $u(a,t)=A\cos\omega t/\omega$ is

$$u(r,t) = \frac{A}{\omega}\frac{J_1(kr)}{J_1(ka)}\cos\omega t \qquad (3.2.3.7)$$

This satisfies the boundary condition and the equation of motion of the elastic material. The steady state solution for u(a,t)=A/ω (a constant for prescribed values of ω) is a solution at zero frequency so one require u(r,t) to satisfy

$$u(a,t) = \frac{A}{\omega} \quad , \qquad \text{independant of time} \qquad (3.2.3.8)$$

$$u(r,t) = u(r) \qquad (3.2.3.9)$$

and

$$\frac{d^2u}{dr^2} + \frac{1}{r}\frac{du}{dr} - \frac{u}{r^2} = 0 \qquad (3.2.3.10)$$

A solution that satisfies these conditions and satisfies u(0)=0 is the linear solution with r

$$u(a,t) = \frac{A}{\omega}\frac{r}{a} \qquad (3.2.3.11)$$

This corresponds to a rigid body rotation of the cylinder through an angle (A/ωa).

For $t < \frac{\pi}{\omega}$ the one has

$$u_1(r,t) = \frac{A}{\omega}\left(\frac{r}{a} - \frac{J_1\left(ka\frac{r}{a}\right)}{J_1(ka)}\cos\omega t\right) + \sum_{i=1}^{\infty}(A_i\cos\omega_i t + B_i\sin\omega_i t)\Phi_i(r) \qquad (3.2.3.12)$$

The solution must satisfy the initial conditions

$$u(r,0) = 0 \qquad (3.2.3.13)$$

$$\dot{u}(r,0) = 0 \qquad (3.2.3.14)$$

Substituting (3.2.3.12) into (3.2.3.13) and (3.2.3.14) one obtains

$$\frac{A}{\omega}\left(\frac{r}{a} - \frac{J_1(kr)}{J_1(ka)}\right) + \sum_{i=1}^{\infty}(A_i\Phi_i(r) = 0 \qquad (3.2.3.15)$$

and

$$\sum_{i=1}^{\infty} B_i\omega_i\Phi_i(r) = 0 \qquad (3.2.3.16)$$

Orthogonality of the modes ($\int_0^a \Phi_i(r)\Phi_j(r)rdr = 0, for, i \neq j$) implies, from (3.2.3.16) that B_i=0. The coefficients Ai are then given by,

$$A_i = \frac{-A}{\omega}\frac{\int_0^a \left(\frac{r}{a} - \frac{J_1(kr)}{J_1(ka)}\right)\Phi_i(r)rdr}{\int_0^a \Phi_i{}^2(r)rdr} \qquad (3.2.3.17)$$

and

$$u_1(r,t) = \frac{A}{\omega}\left(\frac{r}{a} - \frac{J_1\left(ka\frac{r}{a}\right)}{J_1(ka)}\cos\omega t\right) - \frac{A}{\omega}\sum_{i=1}^{\infty}\frac{\int_0^a \left(\frac{r}{a} - \frac{J_1(kr)}{J_1(ka)}\right)\Phi_i(r)rdr}{\int_0^a \Phi_i{}^2(r)rdr}\cos\omega_i t\Phi_i(r)$$

For the second displacement input given in (3.2.3.6), $-\frac{A}{\omega}(1+\cos\omega(t-T)$, one can likewise obtain a solution for zero initial conditions at time t=T.

$$u_2(r,t) = \frac{-A}{\omega}\left(\frac{r}{a} + \frac{J_1(kr)}{J_1(ka)}\cos\omega(t-T)\right) + \sum_{i=1}^{\infty}(C_i\cos\omega_i(t-T) + D_i\sin\omega_i(t-T))\Phi_i(r) \qquad (3.2.3.18)$$

for conditions

$$u_2(r,t=T) = 0 \qquad (3.2.3.19)$$

$$\dot{u}_2(r,t=T) = 0 \qquad (3.2.3.20)$$

one obtains $D_i = 0$

and,

$$C_i = \frac{A}{\omega}\frac{\int_0^a \left(\frac{r}{a} + \frac{J_1(kr)}{J_1(ka)}\right)\Phi_i(r)rdr}{\int_0^a \Phi_i{}^2(r)rdr} \qquad (3.2.3.21)$$

the solution is then,

$$u_2(r,t) = \frac{-A}{\omega}\left(\frac{r}{a} + \frac{J_1(kr)}{J_1(ka)}\cos\omega(t-T)\right) + \sum_{i=1}^{\infty}\frac{A}{\omega}\frac{\int_0^a \left(\frac{r}{a} + \frac{J_1(kr)}{J_1(ka)}\right)\Phi_i(r)rdr}{\int_0^a \Phi_i{}^2(r)rdr}\cos\omega_i(t-T)\Phi_i(r) \qquad (3.2.3.22)$$

The solution for the cylindrical model is then

$u(r,t) = u_1(r,t)$ for $t < \pi/\omega$

and

$u(r,t) = u_1(r,t) + u_2(r,t)$ for $t > \pi/\omega$.

The corresponding strain being obtained using the relationship in equation (3.1.1).

3.3. Numerical Prediction of the Viscoelastic Response for Transient Excitation.

The procedure followed is based upon the Input-Output relationship of linear systems, namely,

$$y(t) = h(t) \otimes x(t) \tag{3.3.1}$$

and,

$$Y(f) = H(f).X(f) \qquad \text{or } Y(\omega)=H(\omega).X(\omega) \tag{3.3.2}$$

where $\otimes$ represents the convolution integral ($\int_0^t h(t-\tau)x(\tau)d\tau$); x(t) and X(ω) are the inputs in the time domain and its Fourier transform; h(t) and H(ω) are the impulse response function and its Fourier transform (known as the transfer function) and y(t) and Y(ω) are the responses in the time domain and its Fourier transform, respectively.

In section 3.1, the transfer functions for the material due to harmonic boundary conditions have been derived. Multiplying these functions by the Fourier transform (spectrum) of the inputs, e.g. for a half sine input velocity on the periphery, and then inverse Fourier transforming one can obtain the response of the material in the time domain. Analytically the Fourier transform of the input can be expressed but the inverse Fourier transform of the material response can only be evaluated numerically for damped (lossy) material using Fast Fourier Transforms.

The case considered in detail is for a half sine velocity input (figure below), as equation 3.2.1.

$$\dot{u}(a,t) = \begin{cases} A\sin\omega_1 t & 0 \le t < \dfrac{\pi}{\omega_1} \\ 0 & \dfrac{\pi}{\omega_1} < t \end{cases} \tag{3.3.3}$$

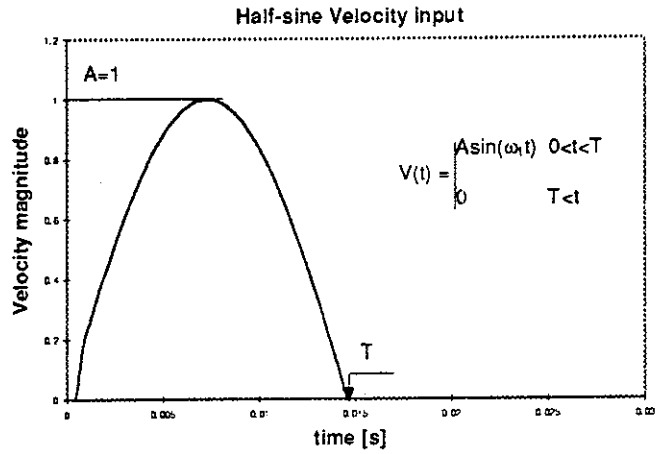

The Fourier transform of the half-sine velocity is given by:

$$V(\omega) = \frac{a\Omega_{max}\omega_1}{\omega_1^2 - \omega^2}\left(1 + e^{-j\pi\frac{\omega}{\omega_1}}\right), \tag{3.3.4}$$

where ω_1 is the input frequency, Ω_{max} =1 for unit angular velocity.

The strain transfer function, $\varepsilon(\omega)$, for a harmonic velocity applied to the boundary is given as equation 3.1.18.

$$\varepsilon(\omega) = -\frac{1}{j\omega}\frac{(ka)J_2\left(ka\frac{r}{a}\right)}{2aJ_1(ka)} \tag{3.3.5}$$

$\varepsilon(\omega)$ is then multiplied by the Fourier transform of the input $X(\omega)$ for the Fourier transform of the strain,

$$\varepsilon(\omega).V(\omega) = -\frac{1}{j\omega}\frac{a\Omega_{max}\omega_1}{\omega_1^2 - \omega^2}\frac{(ka)J_2\left(ka\frac{r}{a}\right)}{2aJ_1(ka)}\left(1 + e^{-j\pi\frac{\omega}{\omega_1}}\right) \tag{3.3.6}$$

The inverse Fourier transform of this quantity gives the strain time history due to the half sine velocity input.

$$\varepsilon(t).= \int_{-\infty}^{+\infty} -\frac{1}{j\omega}\frac{a\Omega_{max}\omega_1}{\omega_1^2 - \omega^2}\frac{(ka)J_2\left(ka\frac{r}{a}\right)}{2aJ_1(ka)}\left(1 + e^{-j\pi\frac{\omega}{\omega_1}}\right)e^{j\omega t}d\omega \tag{3.3.7}$$

For numerical implementation the procedure evaluates expression (3.3.6) for a range of frequency 0 - f_{max} ($\equiv \omega_{max}/2\pi$). The shear wave wavenumber k, frequency dependent for viscoelastic material, is evaluated using the following relationships:

$$k = \frac{\omega}{c} \qquad , c = \sqrt{\frac{G}{\rho}},$$

where G = G(ω) varies with frequency and defined for a Standard model (see section 2.3.2) as:

$$G(\omega) = (K_1 + K_2) - \frac{K_1\omega_d}{\omega_d + j\omega} \text{ where } \omega_d = \frac{K_1}{C_1} \text{ the relaxation frequency.}$$

The inverse Fourier transform, given by equation 3.3.7, is calculated using finite fast Fourier transforms with appropriate scaling due to the number of points in the transform and the sampling rate. The Fast Fourier transform actually processes the data for $0 \le \omega \le \omega_{max}$ with a reflected complex conjugate version defined for $\omega_{max} \le \omega \le 2\omega_{max}$ so that a causal real solution is numerically produced in the time domain. The following results are figures showing the maximum principal strain, equivalent in these cases to the maximum shear strain, as a function of position and non-dimensional time in the cylindrical model. The results are produced from the analysis described here and also shown are the predictions from the FE models for a suitable value of the shear modulii (long term and short term) and an appropriate relaxation frequency.
Generally there are two main comments to note. The FE predictions predict an earlier arrival of the strain then is predicted based on simple wavespeed assumptions and this is more noticeable in the latter figures showing the response nearer to the centre of the model. Secondly the peak values of the strain are lower for the FE results and may be a consequence of there being some energy that has propagated faster in the numerical model, before the time of arrival of the main shear wave.

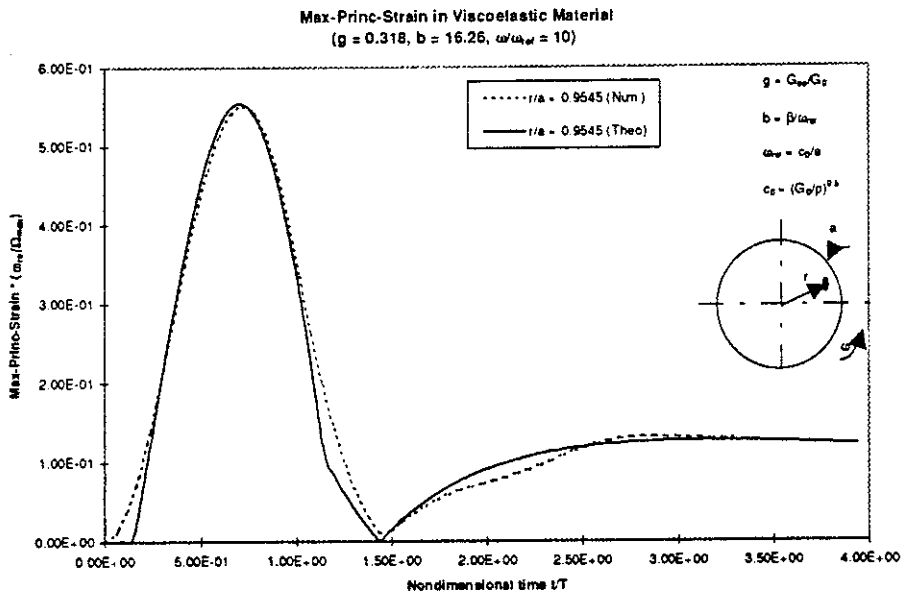

Theoretical max.=0.5537, Numerical (FE) max.=0.5505

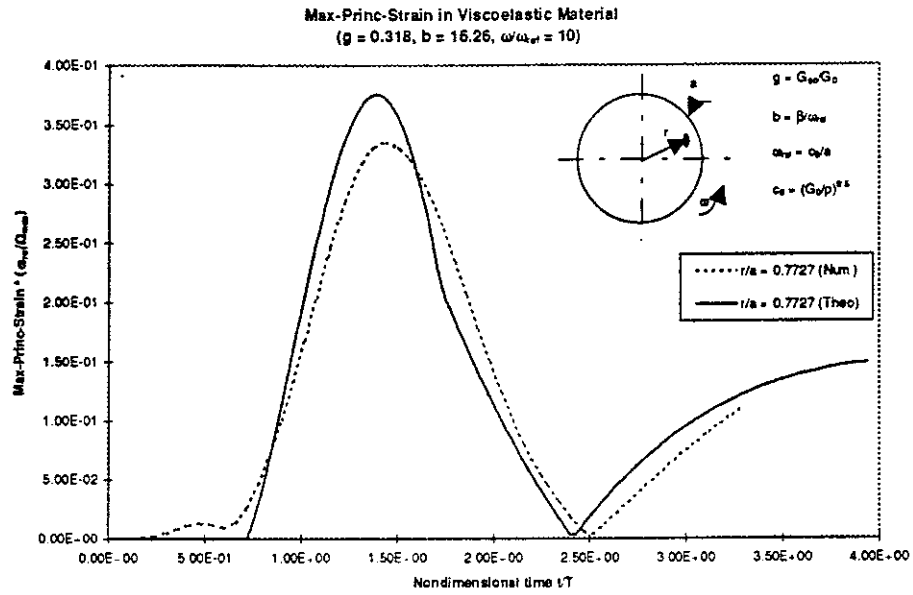

Theoretical max.=0.3751, Numerical (FE) max.=0.3346

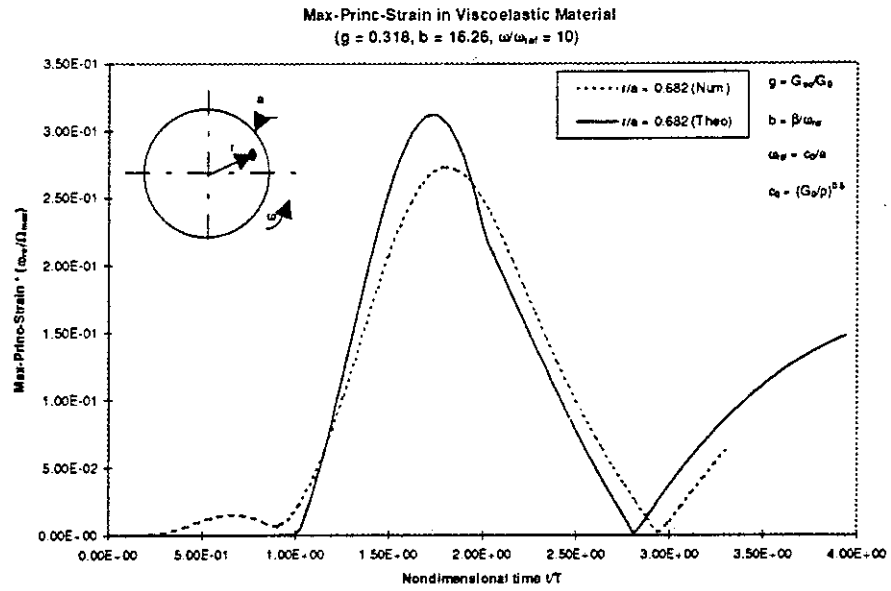

Theoretical max.=0.312, Numerical (FE) max.=0.2727

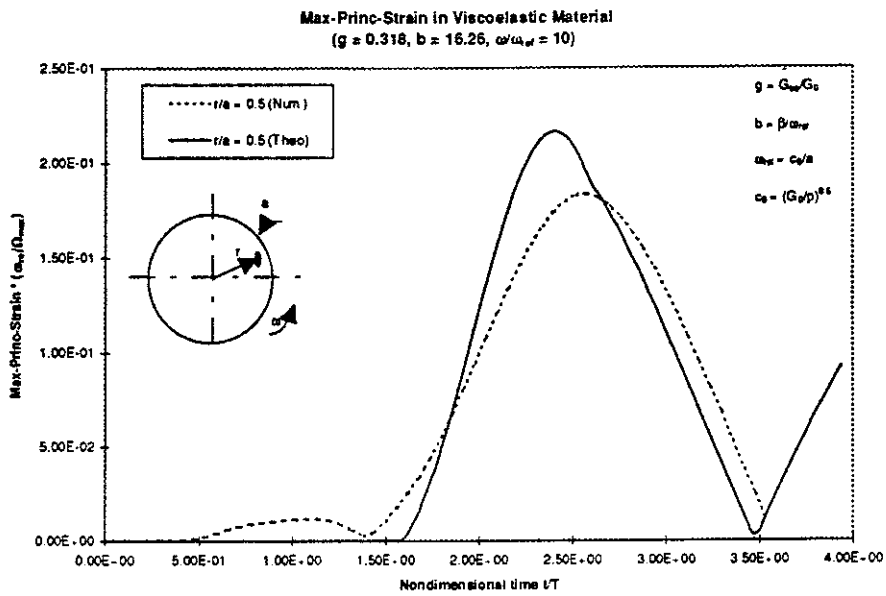

Theoretical max.=0.2162, Numerical (FE) max.=0.18327

4. FE STUDY OF THE DYNAMIC SHEAR RESPONSE OF THE BRAIN

4.1 Cylinder filled with Elastic/ Viscoelastic Materials

4.1.1. *Introduction*

As a first step towards studying the shear response of the brain, A plane strain model, consisting of a simple cylinder filled with a cerebral material was used (figure 4.1.1). The analysis is based on the same assumptions as in the previous section related to the analytical analysis, namely, the no-slip at the boundary (Brain-Skull interface) is assumed and nearly incompressible brain material is used (Bulk modulus Bs=2.083 E09 Pa). As explained previously, the maximum principal strain in the brain matter induced by a half-sine velocity input is of interest. Three models (A, B, and C) have been investigated, and models A and C give the best accuracy, but model A is numerically smaller. Hence, the model A is used in this investigation.

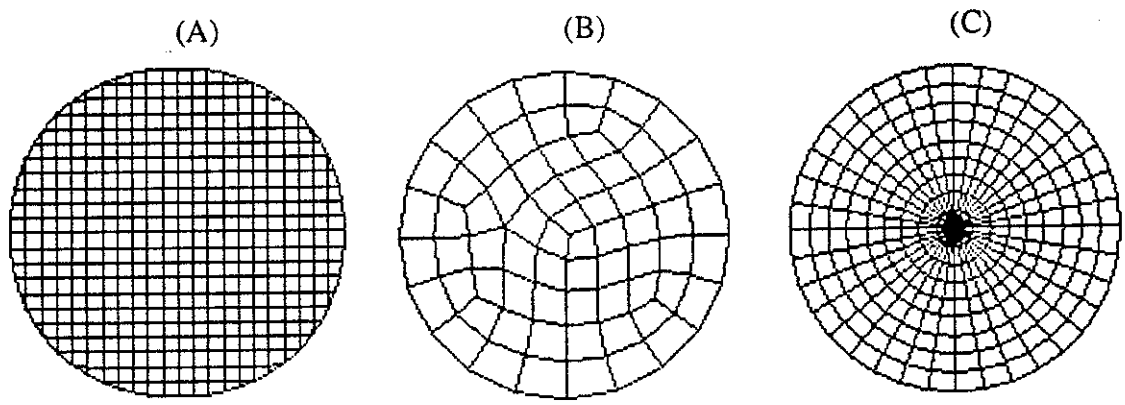

Figure 4.1.1. 2D Finite Element Models used

4.1.2. Scaling

From the differences in shape, size, and properties between animal and human brain material it follows that no direct conclusions regarding tolerance levels for man can be made from animal tests. Thus, scaling techniques have been used to correlate results obtained on animals to the human (Holbourn in 1943, Ljung in 1980, Margulies et al. in 1985). In the present work, scaling used assume that compressive wave effect could not be expected for this geometry and loading type. Hence, the shear strain in the brain at a given point is a function of the following set of parameters,

$$\varepsilon = \varepsilon(t, a, c, \Omega(t), T, \beta, \delta) \tag{4.1}$$

where t denotes time, a radius of the cylinder, $\Omega(t)$ the velocity input, T characteristic time scale of motion, δ is the shear moduli ratio (G_∞/G_0) and β is the viscoelastic decay constant (i.e. $\beta = 0$, and $\delta = 1$ for elastic material).

According to the Buckingham Pi Theorem (cf. Baker et al., 1973) the shear strain ε can be written as a function of a complete set of independent dimensionless groups, formed from the variables and parameters on which ε depends. Dimensional analysis yields that the maximum value (peak) of the shear strain depends on the following parameters,

$$\varepsilon_{max} = \varepsilon\left(\frac{\omega}{\omega_{ref}}, \frac{\Omega_{max}}{\omega_{ref}}, \frac{\beta}{\omega_{ref}}, \delta\right) \tag{4.2}$$

where $\omega_{ref} = c/a$, $\omega = \pi/t^*$ the half-sine velocity pulse fundamental frequency

For an elastic material, the relationship (4.2) is reduced to:

$$\varepsilon_{max} = \varepsilon\left(\frac{\omega}{\omega_{ref}}, \frac{\Omega_{max}}{\omega_{ref}}\right) \tag{4.3}$$

For a fixed angular velocity magnitude Ω_{max}, the relationships above become, for a viscoelastic material,

$$\varepsilon_{max} = \varepsilon\left(\frac{\omega}{\omega_{ref}}, \frac{\beta}{\omega_{ref}}, \delta\right) \tag{4.4}$$

and for an elastic material,

$$\varepsilon_{max} = \varepsilon\left(\frac{\omega}{\omega_{ref}}\right) \tag{4.5}$$

This scaling has been adopted for this investigation.

4.1.3 Non-linear response

To identify possible nonlinear response of the brain, the maximum value reached by the Maximum-Principal-Strain (ε_{max}) is computed for different values of the angular velocity magnitude applied to the cylinder. All simulations have been performed for $\omega/\omega_{ref} = 5$, where ω_{ref} is defined by, $\omega_{ref} = \frac{1}{a}\sqrt{\frac{G}{\rho}}$ for elastic material and by $\omega_{ref} = \frac{1}{a}\sqrt{\frac{G_0}{\rho}}$ for viscoelastic material (i.e. G_o denotes the short term shear modulus).

Figures 4.1.3.1 and 4.1.3.2, show that the dynamic shear response of the brain is linear for a velocity magnitude less or equal to the shear wave propagation speed in the brain ($\Omega_{max} \leq \omega_{ref} = \frac{c}{a}$). The non-linearity appears when Ωmax, the imposed angular velocity, become greater than the shear wave speed in the circumferential direction.

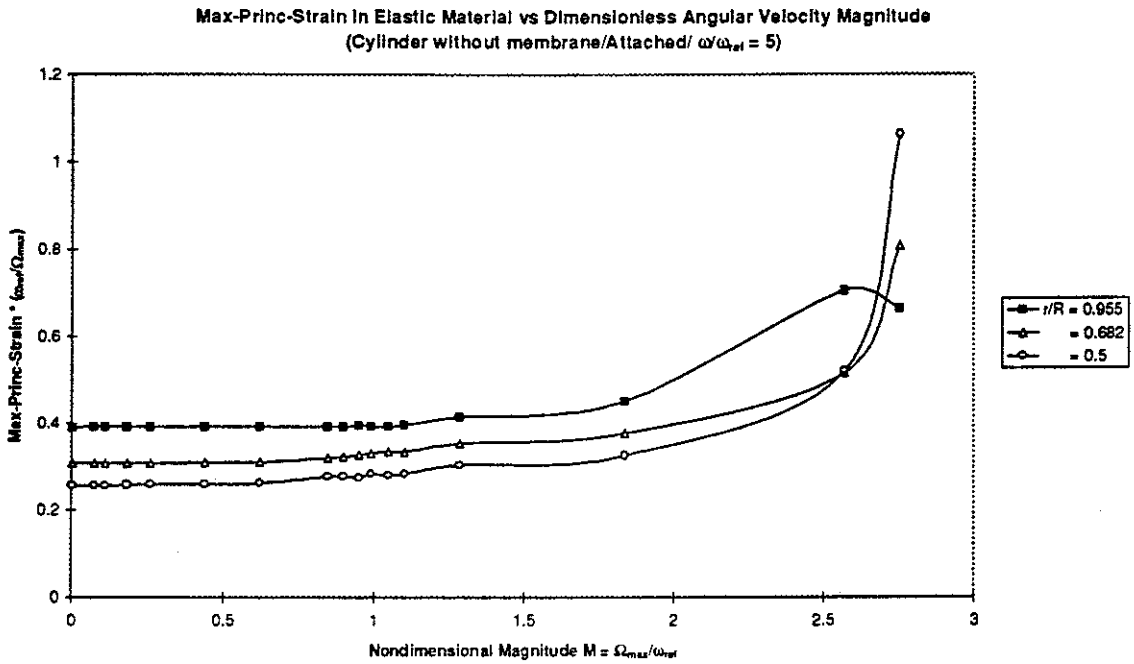

Figure 4.1.3.1. Maximum principal Strain in Elastic Material vs. Dimensionless Angular Velocity Magnitude $M=\Omega_{max}/\omega_{ref}$, with $\omega/\omega_{ref} = 5$

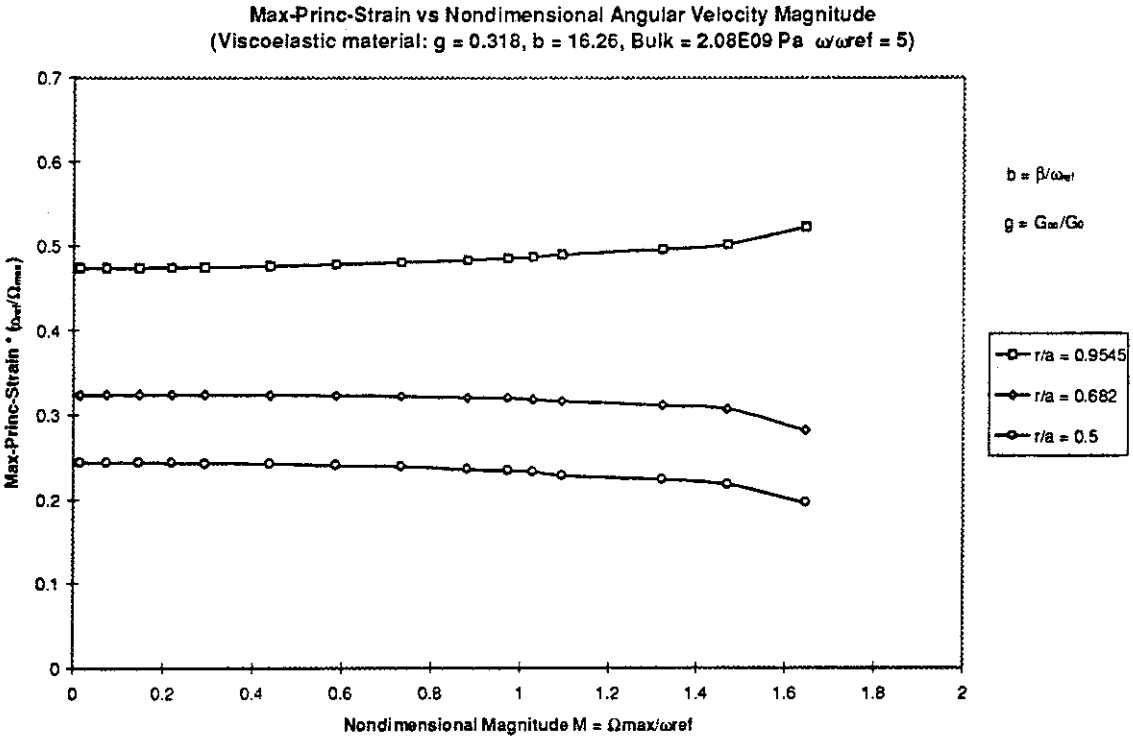

Figure 4.1.3.2. Maximum principal Strain in Viscoelastic Material vs. Dimensionless Angular Velocity Magnitude $M=\Omega_{max}/\omega_{ref}$, with $\omega/\omega_{ref} = 5$

The effect of the relaxation decay is illustrated by figure 4.1.3.3. In fact, this decay has a noticeable effect when it is ten times greater than the natural frequency of the shear wave in the material, i.e.b=β/w_{ref}>10. For b<10 the solution obtained is not significantly different than the elastic solution. Figure 4.1.3.4, shows that the shear strain is very sensitive to the ratio $g=G_\infty/G_0$ and "b". The maximum values of the strain are proportional to the relaxation decay and inversely proportional the shear modulus ratio.

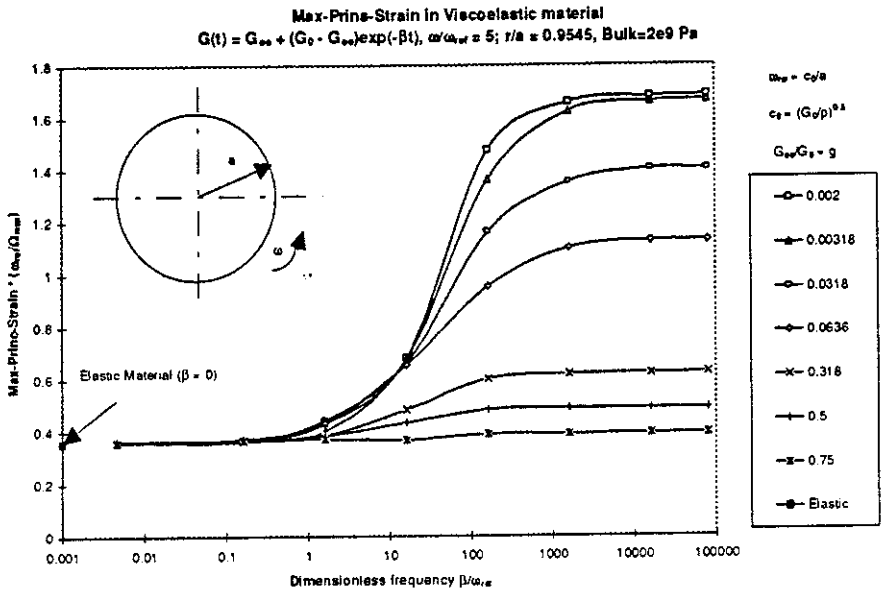

Figure 4.1.3.3: Effect of the Relaxation Decay on Maximum Principal Strain in Viscoelastic Material

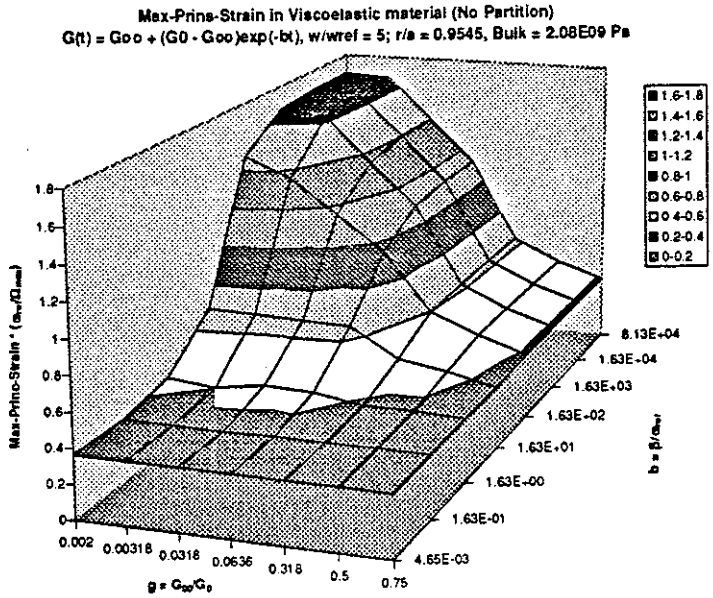

Figure 4.1.3.4: Contour plot of on Maximum Principal Strain in Viscoelastic Material vs. Dimensionless Relaxation Decay and Dimensionless Shear Modulus.

Particular cases are shown in figure 4.1.3.5, which illustrates the evolution of the strain with respect to the duration of the loading (i.e. $T_{ref}/T=\omega/\omega_{ref}$), for elastic material, viscoelastic materials (i) LSBM data , Turquier 1996) and (ii) ISVR data obtained by model fit to the data from Shuck (see figure 2.2). This figure shows that LSBM data characterised by "b=1.626" agrees well with the elastic solution. The effect of the relaxation is insignificant. However, the ISVR curve shows that the relaxation has a significant effect on the strain in the brain. Moreover, it indicates that the brain is more sensitive to the low frequency contribution (ω/ω_{ref} <6), (i.e. in this example, ω_{ref} = 16.2). This result is in agreement with previous work by Willinger et al. 1995, when discussing the rotation-translation duality in head trauma. They reported that the mechanism of the diffuse axonal injury (DAI) which is a result to exceeding a certain value of strain in the cerebral tissue, is related to the loading spectrum energy and thus to the duration of loading.

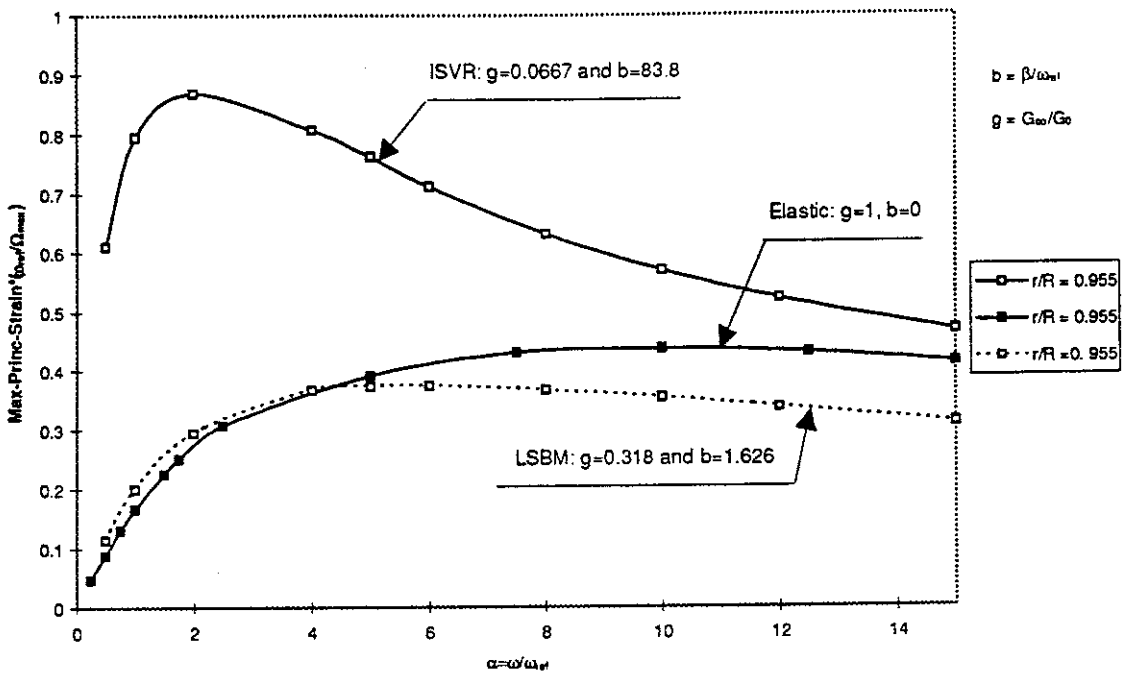

Figure 4.1.3.5: Maximum Principal strain reached in the brain for different materials

One can observe that previously published values of "b" and "g", used in finite element modelling, vary over the range 1.6-21 for "b" and 0.318-0.5 for g. From this parametric study, one should take care when interpreting their results. Furthermore, this study shows the need to conduct more experiments on brain tissue to evaluate its mechanical properties (i.e. the shear modulus components (G_0, G_∞ and β)). It is premature to discuss human tolerance limits until human brain tissue properties are well determined.

4.2 Cylinder with Fixed Rigid Partition filled with Elastic/ Viscoelastic Material

The model studied here is shown in Figure 4.2.1, characterised by introducing a rigid partition and a non viscous fluid between the partition and the brain. A sliding condition is assumed everywhere, namely, at the boundary, between the material and the skull (cylinder), between the fluid and the rigid partition and between the fluid and the brain.
These entities were connected through a contact prescription (contact surface) implemented in the FE code to release under pre-specified tensile and shear loading levels. The contact surfaces used here can be separated, but at any case cannot be penetrated (no penetration between surface(i) and surface(j) is possible). An Arbitrary-Lagrangian-Eulerian formulation is assumed to the fluid elements, with the possibility of auto-smoothing the mesh when it is very distorted. This possibility

is very useful, since the fluid has no resistance to shear, and hence the mesh of the fluid elements will, as expected, become very distorted.
In discretizing the model, specific care has been taken to ensure a high mesh density around the regions where the largest strains are expected to develop. These include the brain skull interface and at the regions of the brain adjacent to the partitioning membrane which were believed to be exhibiting large strains (see figure 4.2.4).

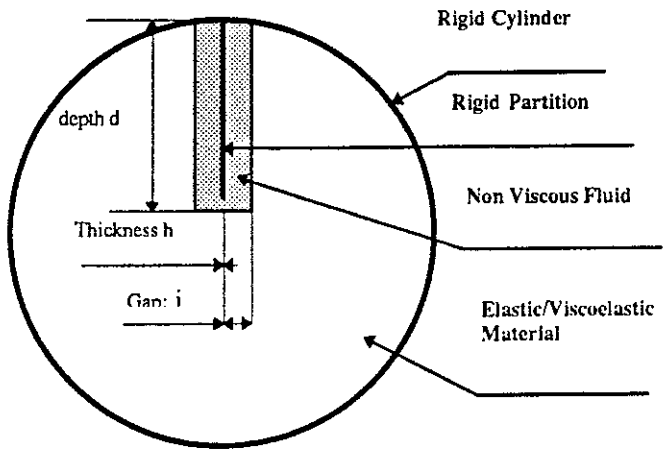

Figure 4.2.1: Schematic Model with Rigid Partition Fixed to the Cylinder,

4.2.1. Influence of fluid physical properties

As expected, the maximum value of strain in the brain is located at the tip of the partition (or Falx in the human head). As shown in figure 4.2.1.1 and figure 4.2.1.2, the physical properties of the fluid, namely the density and the bulk modulus, have no significant effect on the dynamic shear response of the brain. This conclusion assumes that the bulk modulus and the density of the brain are very close to those of the fluid. having limited this investigation to the following ranges:

$$0.5 < B_f/B_s < 5 \qquad \text{and} \qquad 0.8 < \rho_f/\rho_s < 1.2$$

In the following simulations, the bulk modulus and density ratios will be fixed to unity, namely $B_f/B_s = 1$ and $\rho_f/\rho_s = 1$.

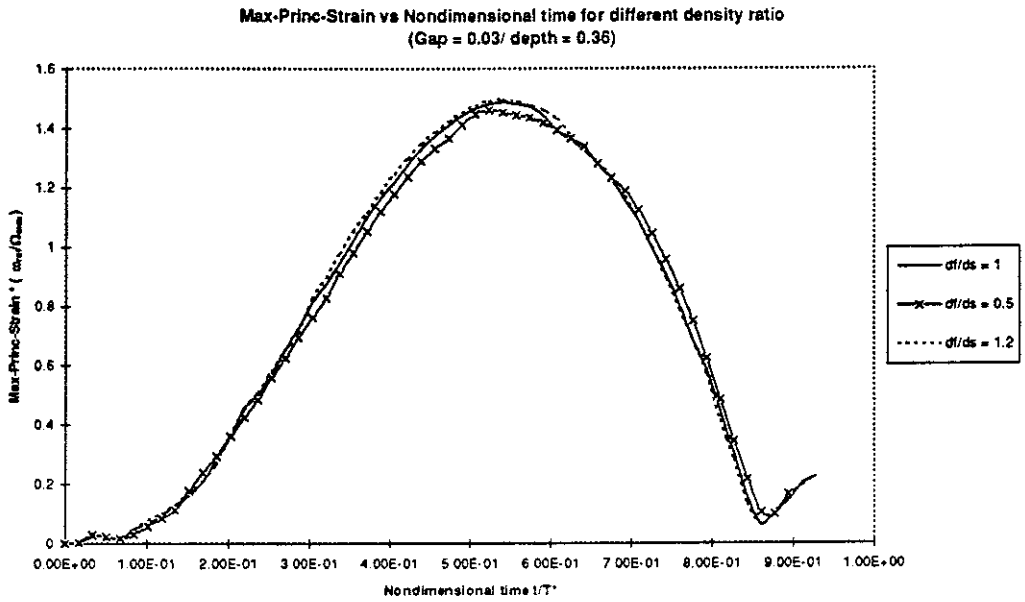

Figure 4.2.1.1: Max. Principal Strain for different density ratio

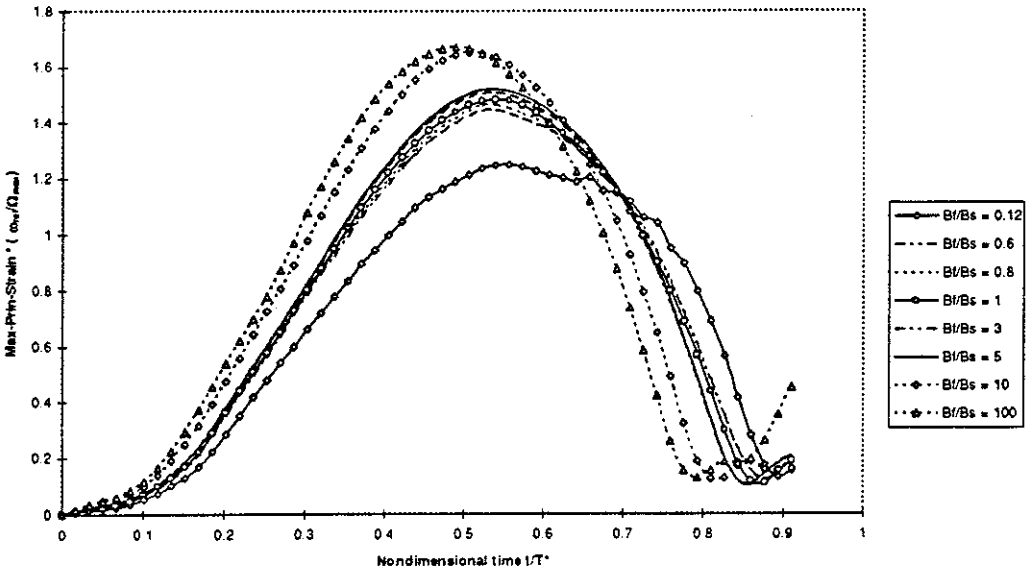

Figure 4.2.1.2: Max. Principal Strain for different bulk modulus ratio

4.2.2. Influence of the Gap

The effect of the gap was elucidated by increasing the gap from j=J/a=0 to 0.06. As shown in figure 4.2.2.1. Further care was taken when meshing the region around the partition and the fluid, where the maximum values of strain are expected. This study will be more focussed on the gap j=0.03, since this value corresponds closest to the human anatomy.

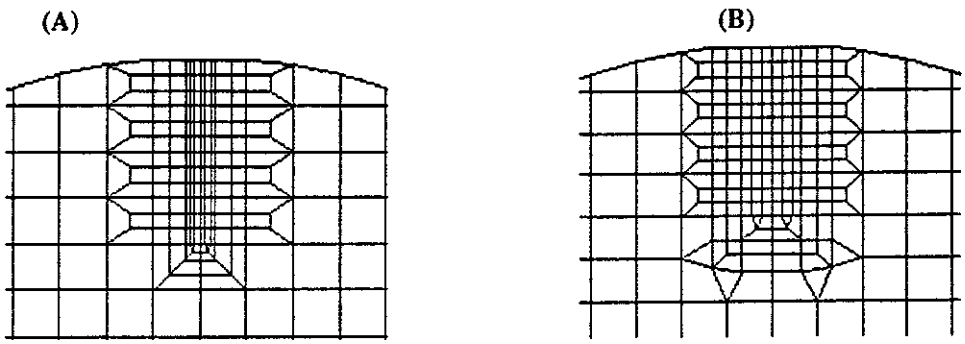

Figure 4.2.2.1. Zoom on the Mesh around the Rigid Partition
(A) gap=0.03, (B) Gap = 0.06

It is observed that the peak Max. principal strain in the brain moves around the tip of the partitioning membrane as shown in figures 4.2.2.2 and 4.2.2.3.
Generally, for the elastic material, the maximum value is reached for a zero gap (j=0), when the brain is in contact with the partition (Falx). The special case when the loading frequency is very low(i.e. quasi-static), the gap increases the strain level, but this difference is not very significant.

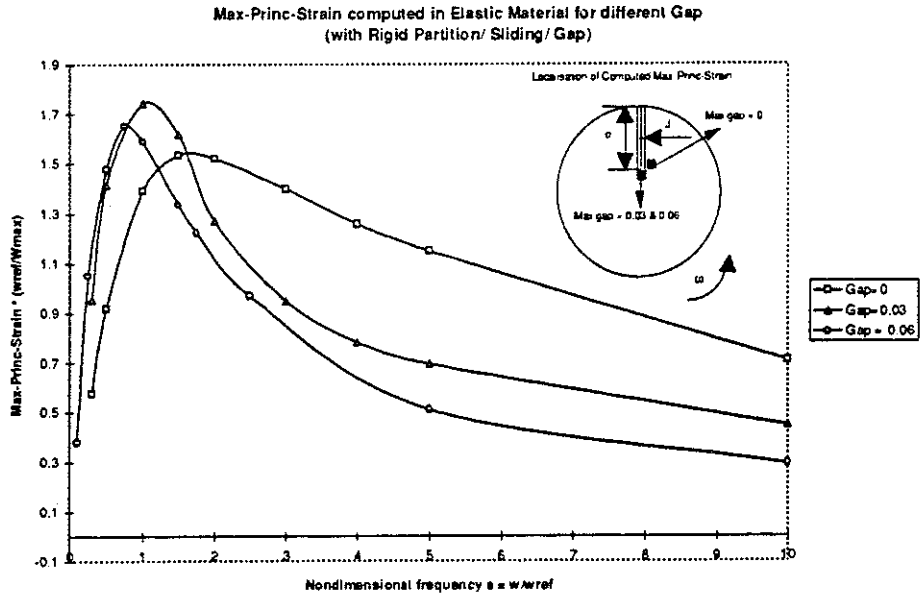

Figure 4.2.2.2. Maximum Value Reached by the Maximum Principal Strain in Elastic Material for Different Gap.

However, for the viscoelastic material, the gap has a strong effect on the strain in the brain by decreasing the strain level. As mentioned above, the strain is very sensitive to the loading at low frequency or long duration loading (see figures 4.2.2.2 and 4.2.2.3).

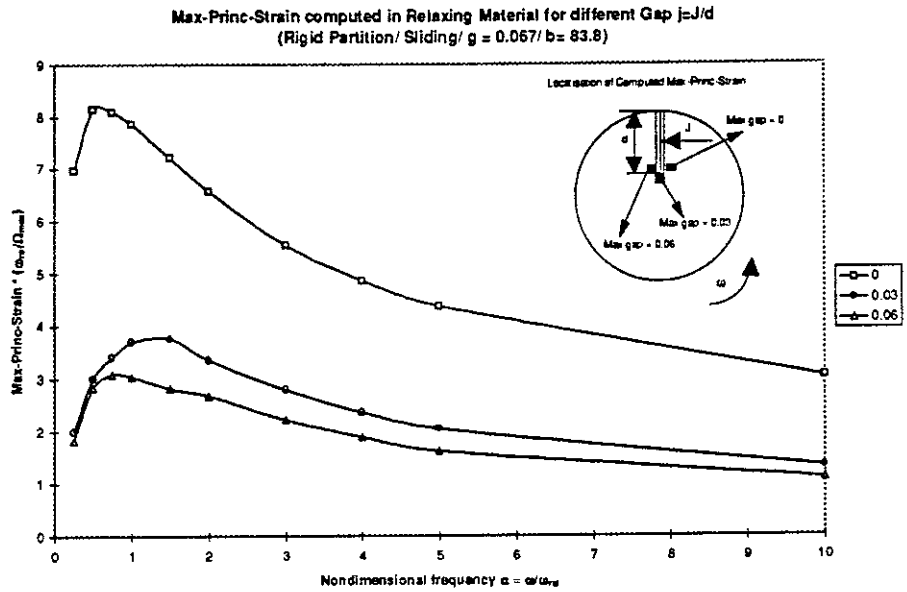

Figure 4.2.2.3. Maximum Value Reached by the Maximum Principal Strain in Viscoelastic Material for Different Gap.

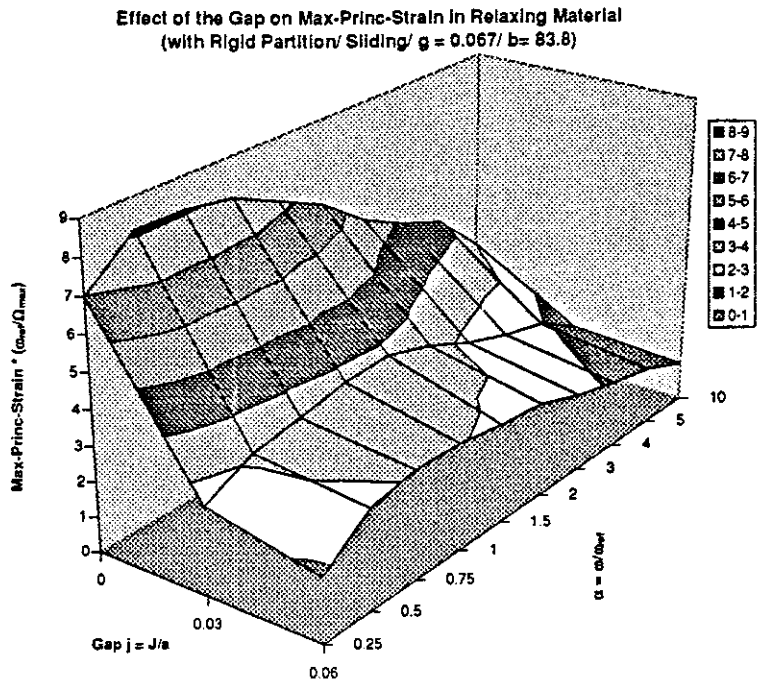

Figure 4.2.2.4. Contour plot of Maximum value reached by the Max. Principal Strain in Viscoelastic Material for Different Gap.

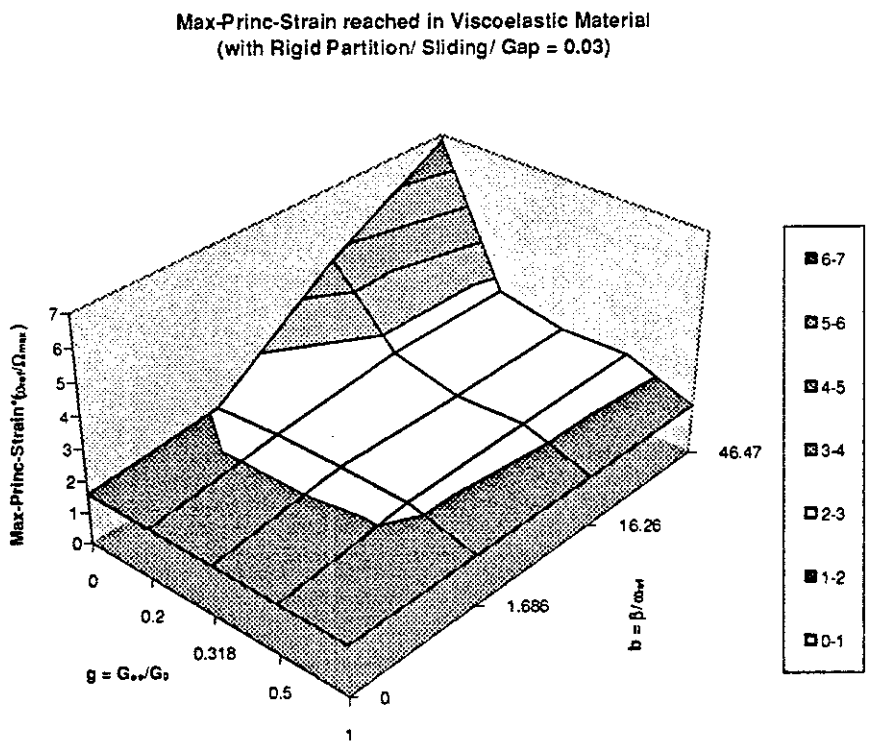

Figure 4.2.7. Contour plot of Maximum value reached by the Max. Principal Strain in Viscoelastic Material (Gap = 0.03)

4.2.3. Influence of the Partition Penetration Depth

Figure 4.2.3.1 shows the mesh refinement for two different partition depths, showing the increased mesh density necessary for a doubling of the depth.

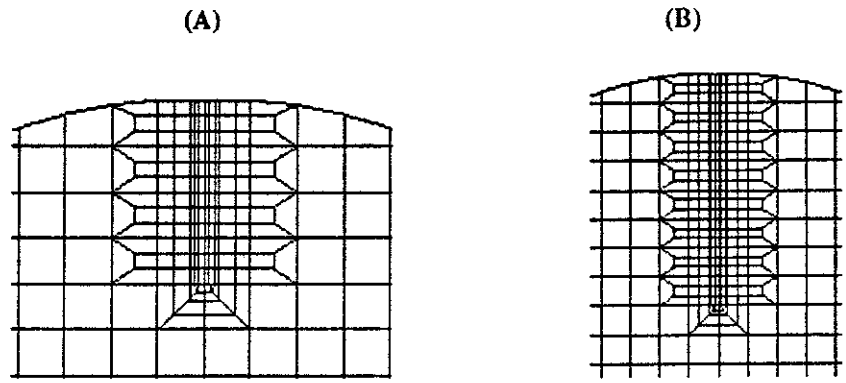

Figure 4.2.3.1: Illustration of Different Partition Depth, (A) δ=0.36, (B) δ=0.73

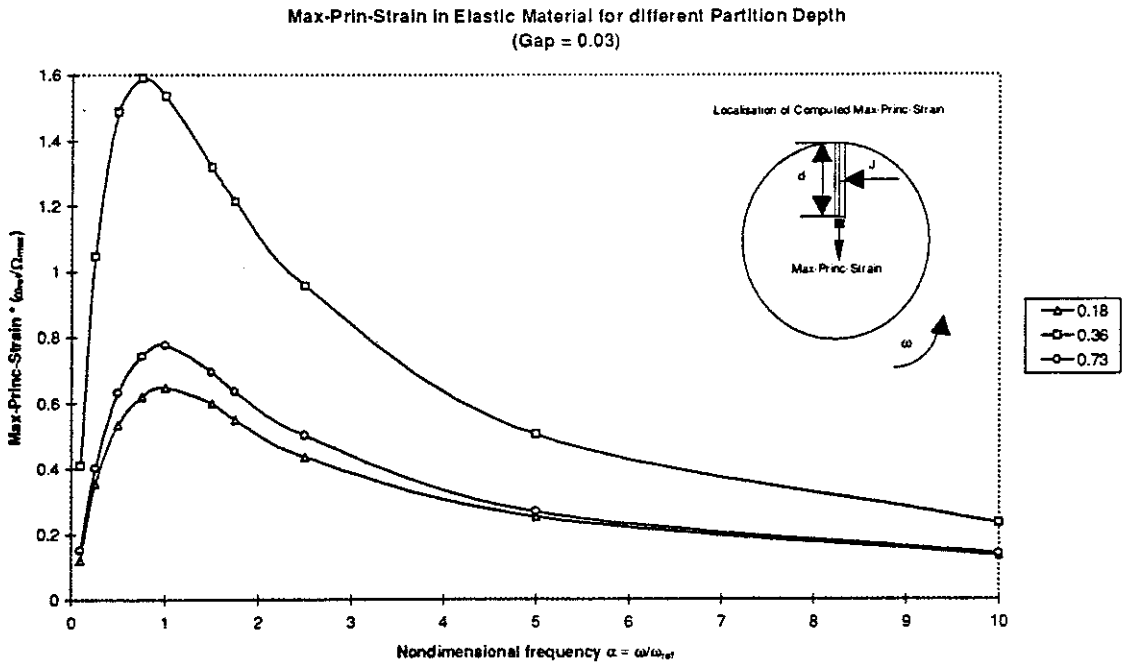

Figure 4.2.3.2 Variation of the Max. Principal strain as a function of the depth of the partition and the duration of the applied load.

Figure 4.2.3.2 is typical of the results for the effect of the penetration depth for a fixed gap size and for a range of loading duration for elastic material. The maximum strain response is not, as might be expected, corresponding to the maximum depth of the partition but is somewhere in between the minimum and maximum values possible. The response has both shear and direct strain components in the general case and probably, as the partitition depth increases, the results tend to a predominantly shear strain response. It is also worth noting that the location of the maximum response is always at the tip of the partition. A similar effect is shown in figure 4.2.3.3 for the viscoelastic material and, apart from the difference in the magnitude of the strain, the characteristics are very similar.

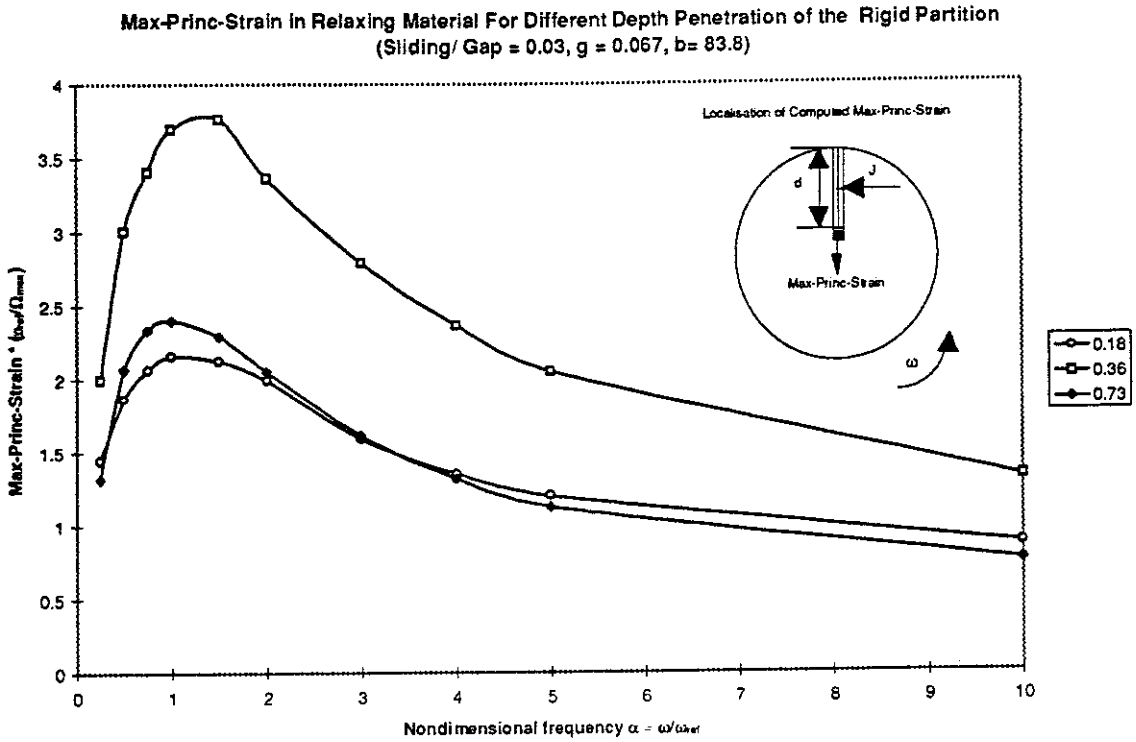

Figure 4.2.3.3 Variation of the Max. Principal strain as a function of the depth of the partition and the duration of the applied load for relaxing material.

4.2.4 Influence of the Fluid at the Container-Material Interface

The effect of the CSF fluid has been considered by modelling a partitition with a gap, as previously described, and introducing fluid elements inbetween the parttion and the cerebral material and between the skull and brain. A thin layer of a non viscous fluid between brain and skull has been introduced (see figure 4.2.4.1). This configuration is the most realistic and representative to the human head. The fluid here has a Bulk modulus of 2.08 MPa and density of 1040 Kg/m3. This fluid has no resistance to shear.

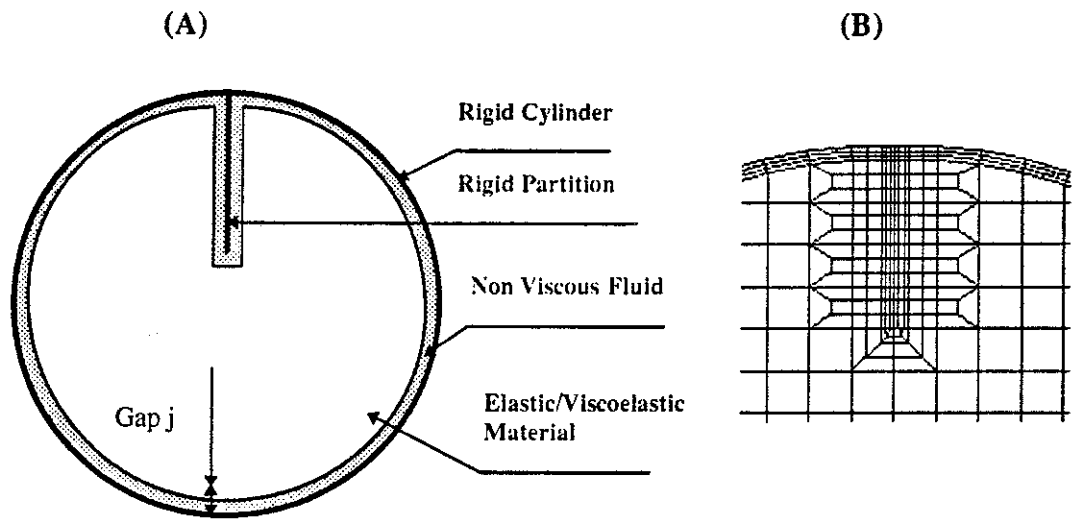

Figure 4.2.4.1: (A) Schematic Model with Rigid Partition with Fluid all around the Elastic/Viscoelastic Material, (B) Zoom on the Mesh around the Sensitive Regions

The effect of this layer, illustrated by figures 4.2.4.2 and 4.2.4.3 for elastic and viscoelastic material models, is characterised by a reduction of the strain level in the brain as expected. This effect is more significant in the case for elastic material than in viscoelastic one (i.e. 25% in elastic material vs. 8 % in viscoelastic material). One can notice, as mentioned in previous sections, that the dynamic response of the brain in shear reaches its maximum value for the excitation frequency close to the frequency of shear wave propagation in the brain.

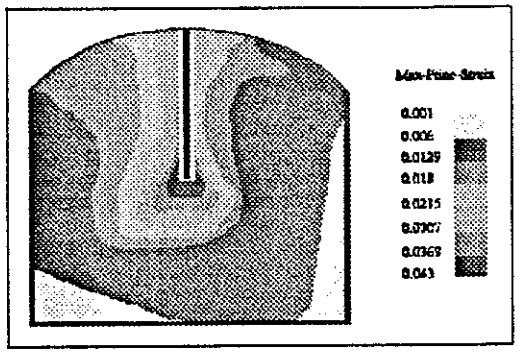

Figure 4.2.4.4a: Contour of maximum principal strain at 20 ms under 50 ms half-sine pulse duration. Note that the maximum value is reached at the tip of the Falx where Diffuse Axonal Injury is very frequent (figure 4.2.4.4b) in case of rotational loading

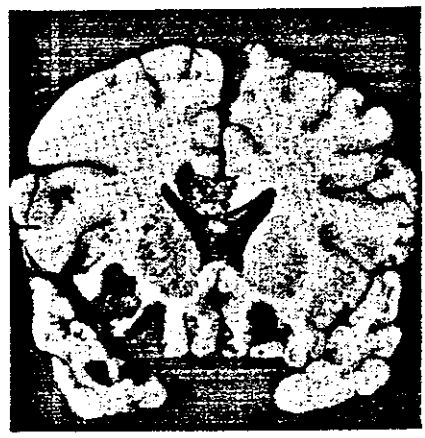

Figure 4.2.4.4b: Laceration of corpus callosum, septum and formix. Motor vehicle accident (Kirkpatrick 1984)

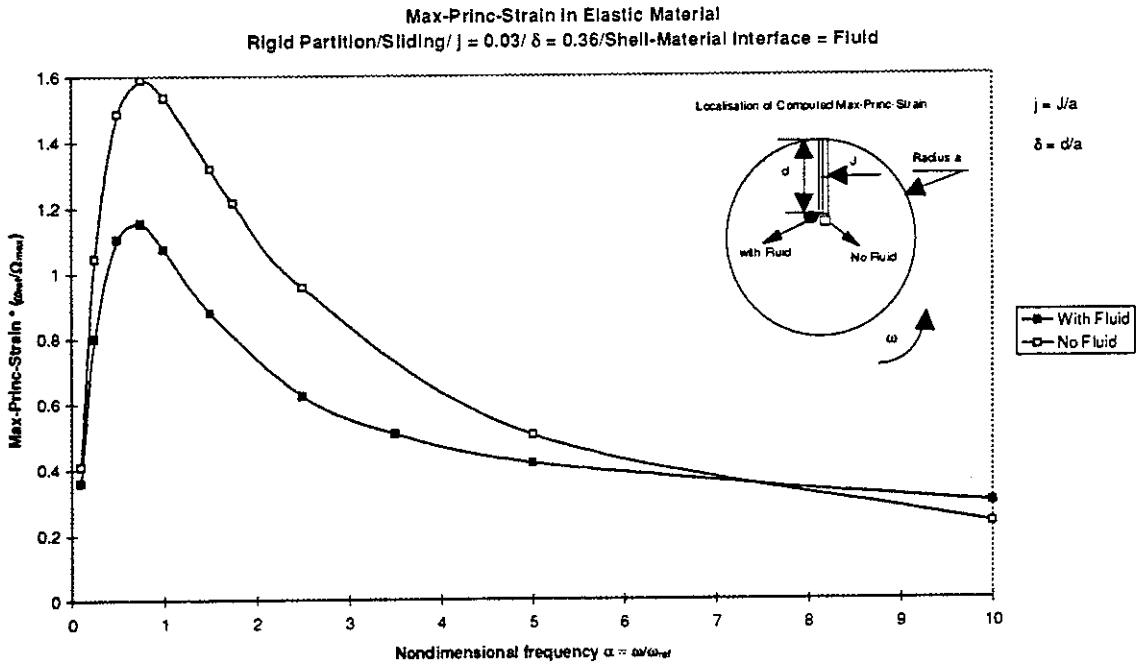

Figure 4.2.4.2. Illustration of the effect of the fluid at the brain-skull interface on maximum principal strain in elastic material

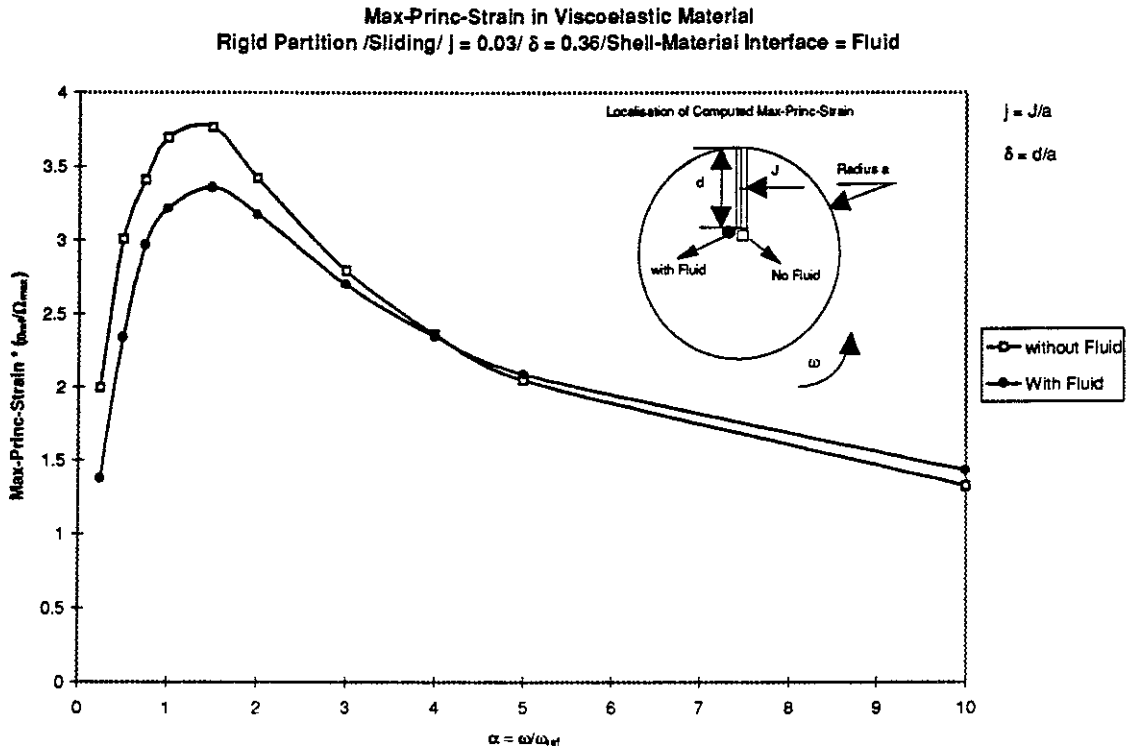

Figure 4.2.4.2. Illustration of the effect of the fluid at the brain-skull interface on maximum principal strain in viscoelastic material

4.3.1. Hinged Rigid Partition with Spring

Additional complexity has been introduced by considering the partition as rigid but being hinged at its connection with the skull. This is a step in the progression in the modelling to introduce flexibility to the partition, representing the Falx. Figure 4.3.1 shows the introduction of the rotational stiffness.

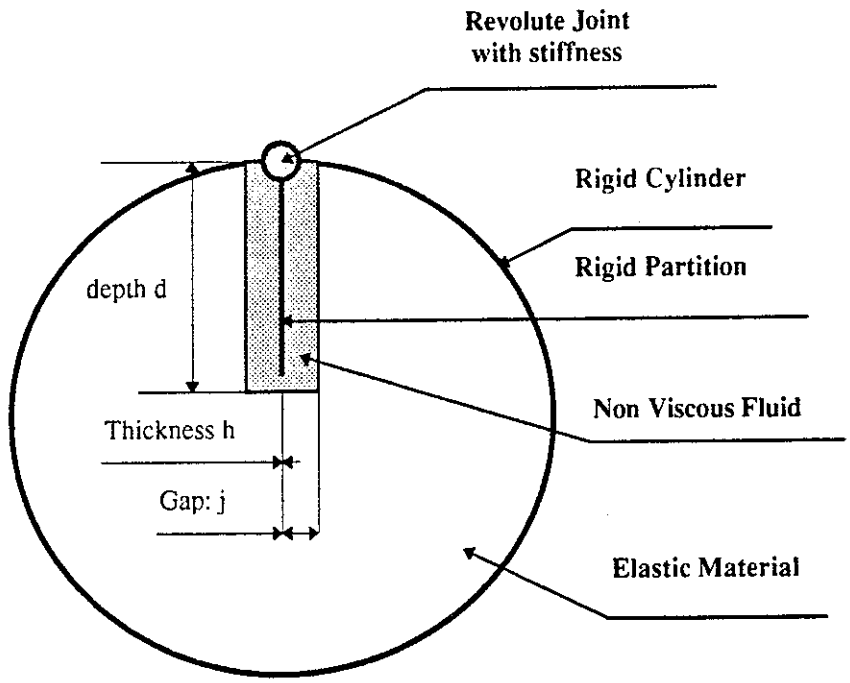

Figure 4.3.1: Model with Hinged Rigid Partition with Spring

For high spring stiffness, greater than 1.0e07 Nm/rad, the results are as if the partition is securely attached to the skull. As the stiffness is reduced, see the results given in figure 4.3.2, there must be rotation of the partition about the pivot and this consequently leads to a reduction of the peak values of the Principal strains. The peak strains are still calculated near to the tip of the partition and figure 4.3.3 illustrates the variation of the peak strains as a function of the spring stiffness (non-dimensionalised against the stiffness of the elastic material).

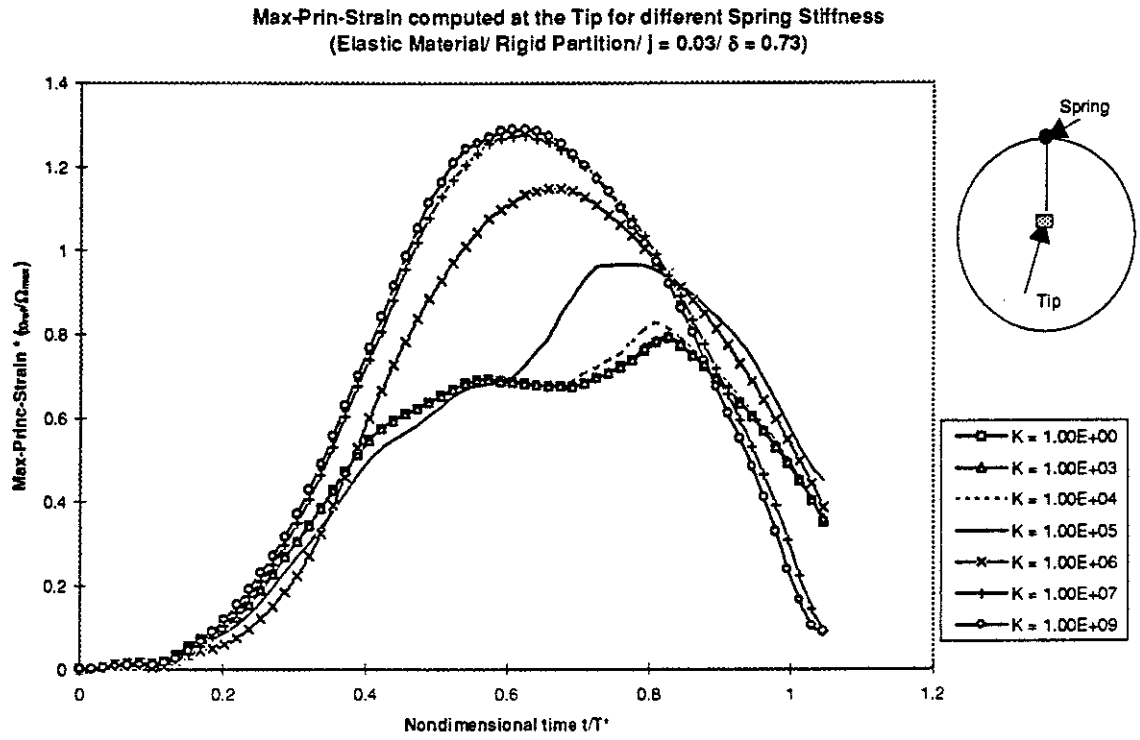

Figure 4.3.2: The Max. Principal Strain in elastic material due to the introduction of a rotational spring at the base of the partition.

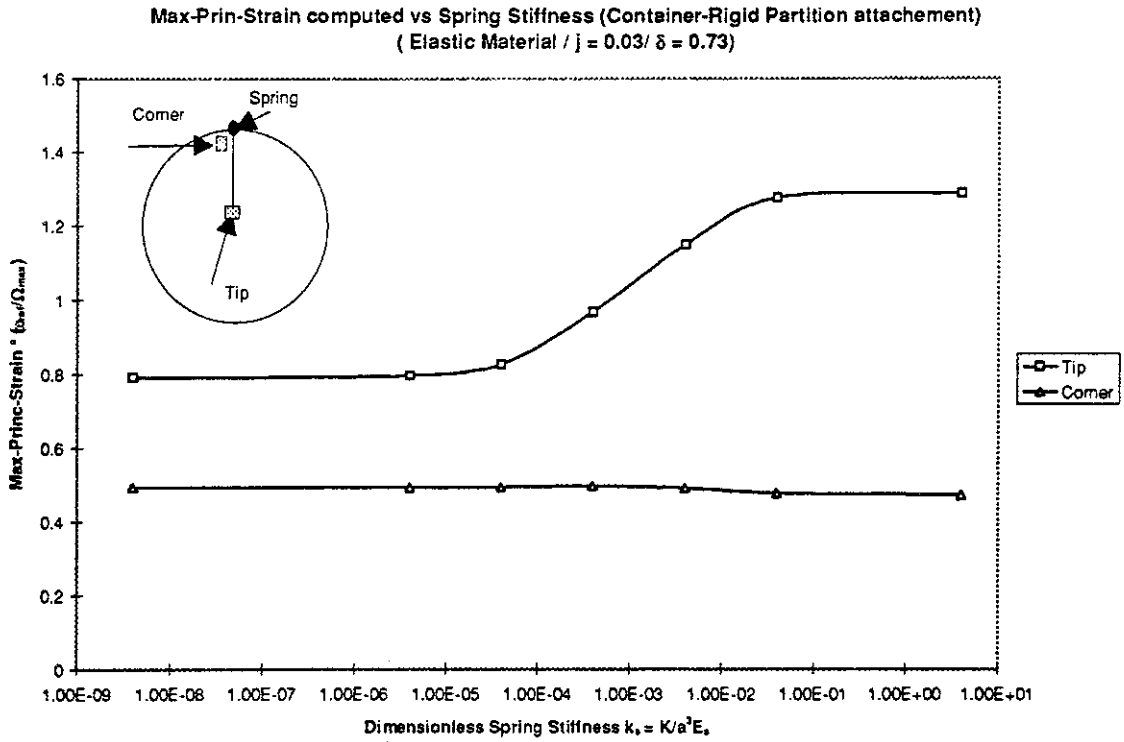

Figure 4.3.3 Variation in the peak strain at the tip and near the base of the partition for rotational spring at the base.

4.3.2 Flexible Partition Attached at its ends

The partition flexibility can be included in two ways. Either one can consider the partition to have negligible bending stiffness and the stiffness that it possess to be due to membrane restoring forces. The second alternative is to assume that the partition has significant thickness and bending stiffness associated with it. As the thickness increases the bending stiffness increases in proportion to the third power of thickness.
The effect of the partition stiffness is given in figure 4.3.4 and compared against the membrane stiffness for the same dimension partition in figure 4.3.5. Increasing the stiffness of the partition produces more deformation in the cerebral matter and the bending stiffness produces approximately double the peak strain, figure 4.3.5, compared to a partition exhibiting membrane stiffness only. The results tend towards the reponse for a completely rigid partition as the stiffness is further increased, see figure 4.3.6, and are as one would expect.

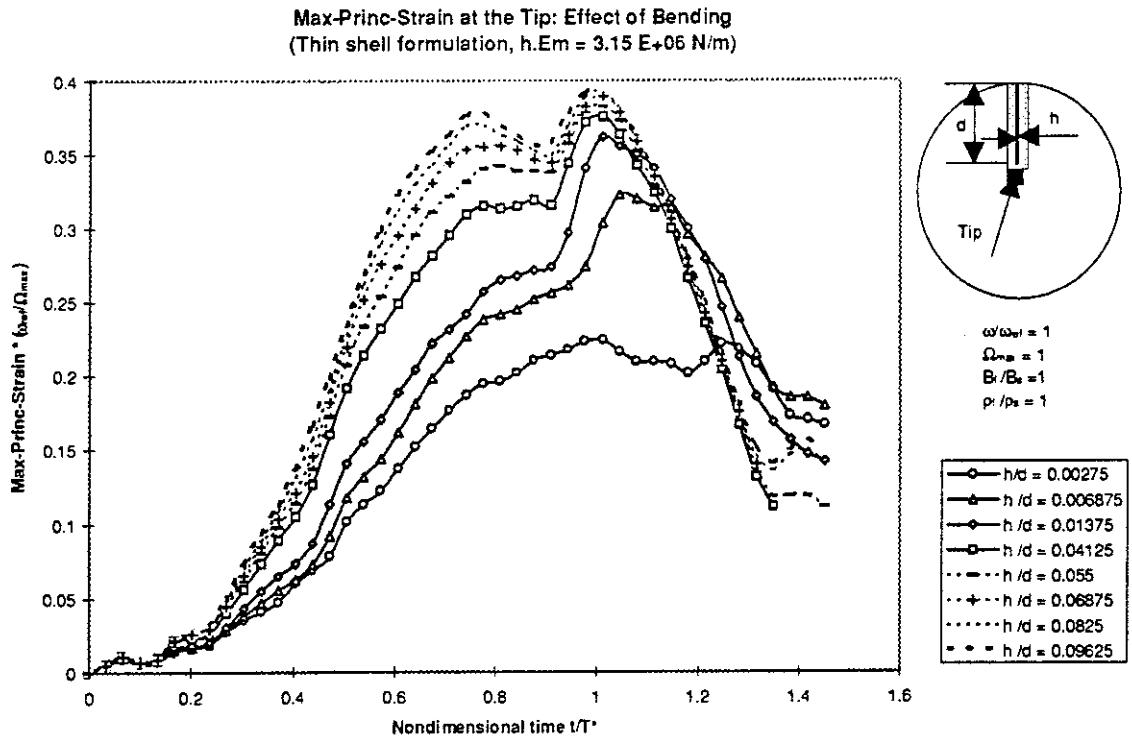

Figure 4.3.4 The effect of the bending stiffness of the partition. Increasing values of h corresponding to increased bending stiffness.

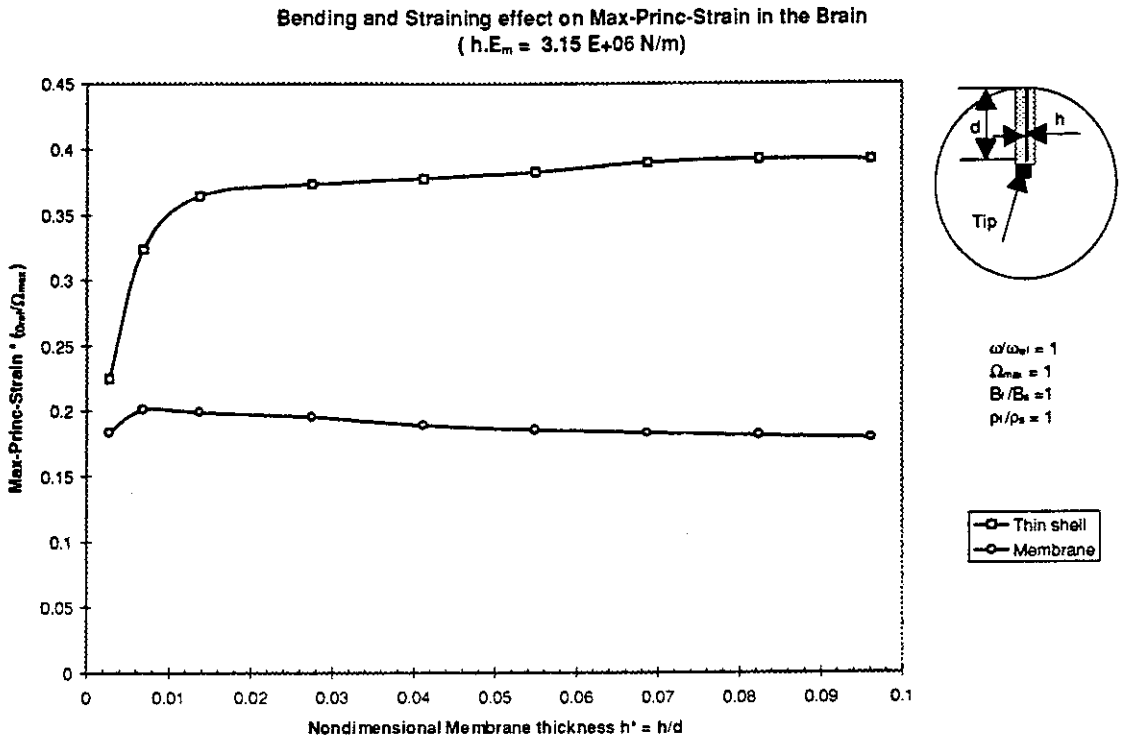

Figure 4.3.5 The effect of the bending stiffness(using thin shell elements) versus the membrane stiffness of the partition on the Principal Strain as a function of the membrane thickness.

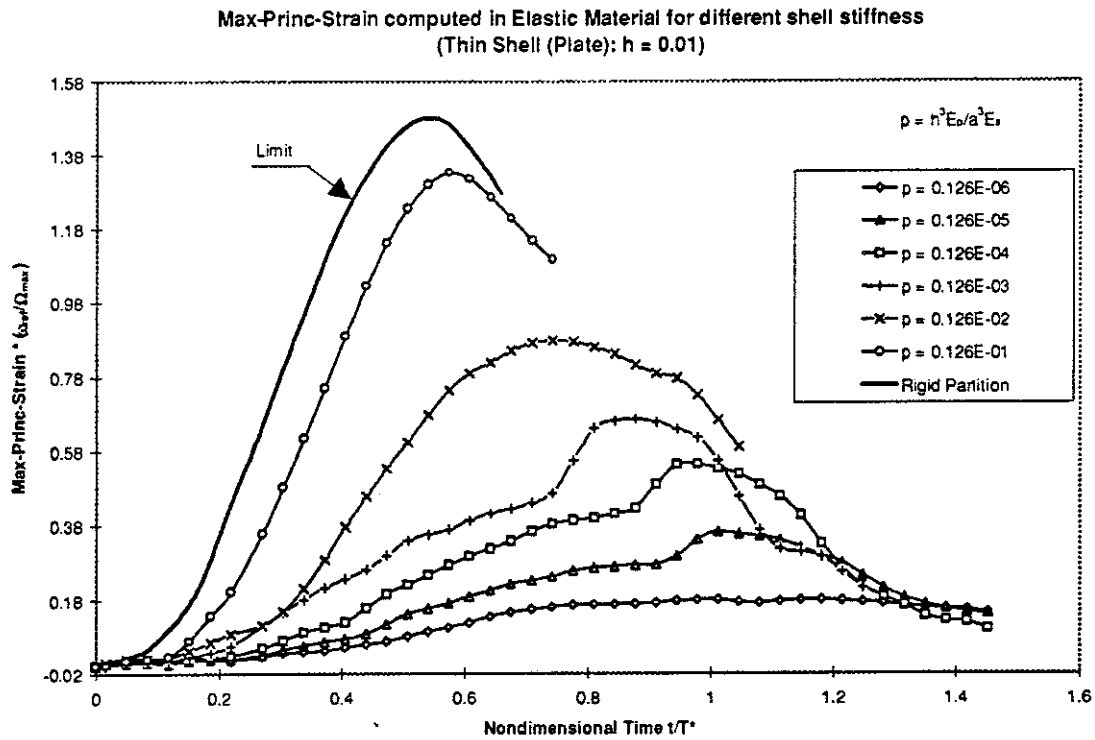

Figure 4.3.6: The increase in peak strain with increasing bending stiffness of the partition .

Similarly, using membrane elements for the partition, simulations have been performed for increasing membrane stiffness and, as in the case for increased bending stiffness, the strain is increased. Figure 4.3.7 for membrane stiffness can be compared with figure 4.3.6 for bending stiffness changes.

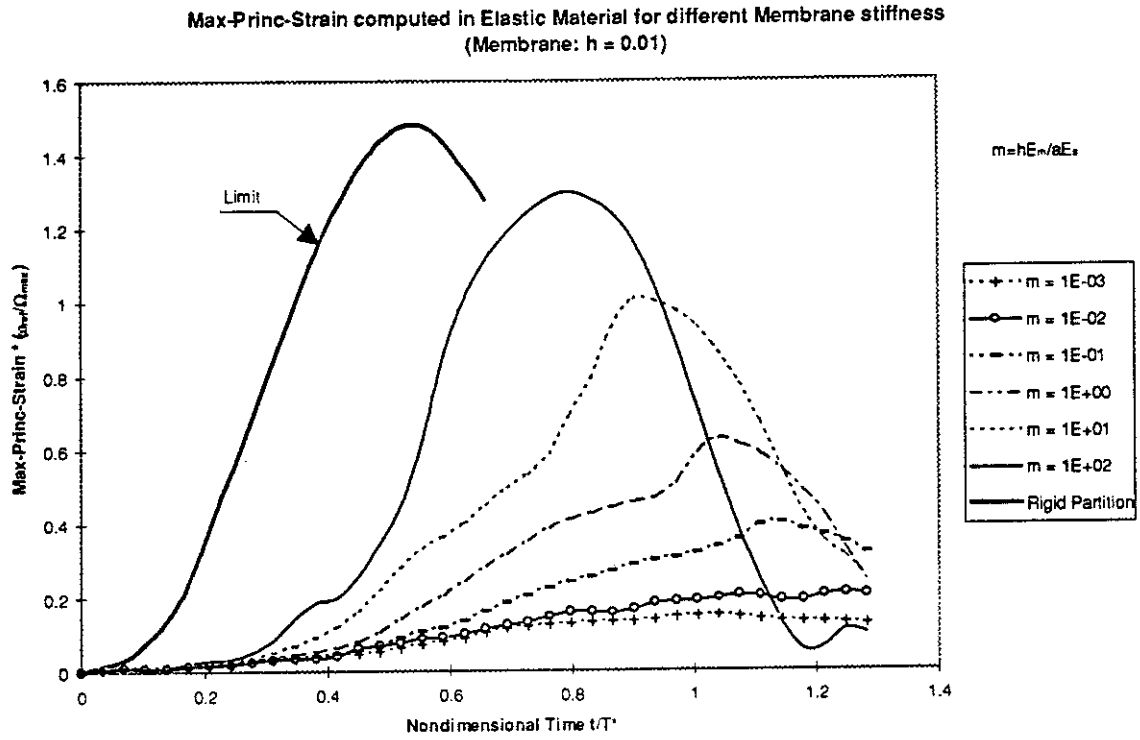

Figure 4.3.7: The effect of increased membrane stiffness of the partition

Graphs of the peak values of the Principal strains are given in figures 4.3.8 and 4.3.9 and show the variation as the stiffness is increased. Likewise increasing the partition stiffness, by changing the modulus of elasticity, produces a similar result for fixed values of partition thickness (see figure 4.3.10).

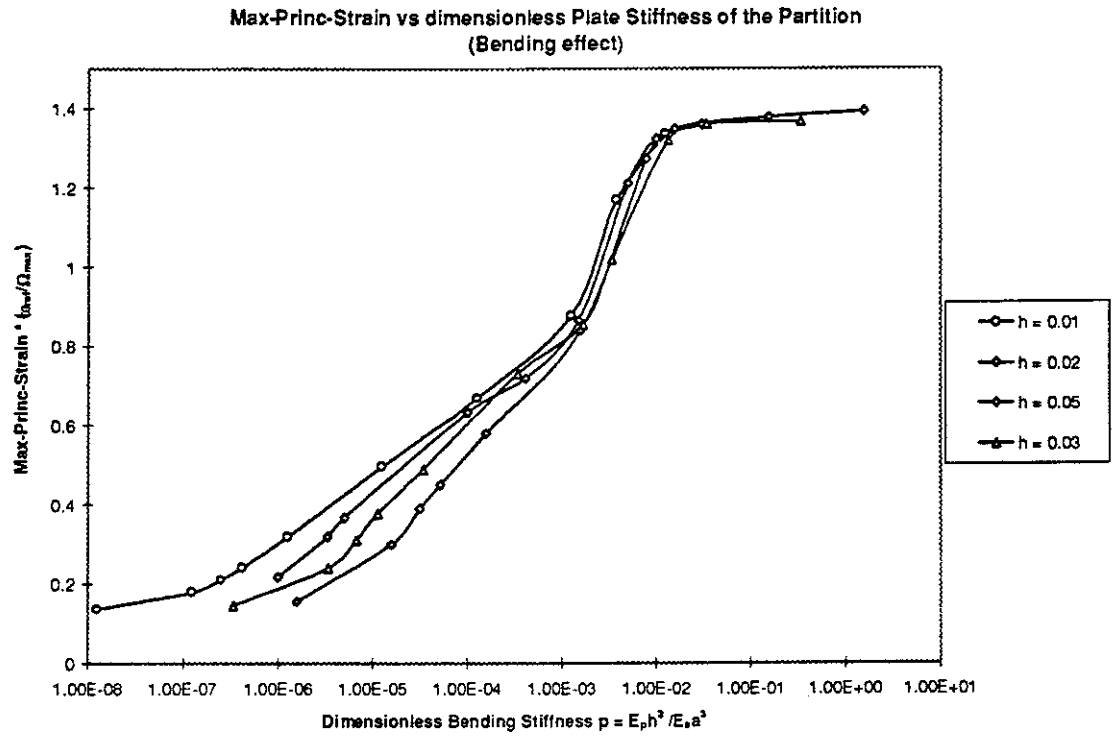

Figure 4.3.8: Peak value of the Max. Principal Strain vs partition bending stiffness

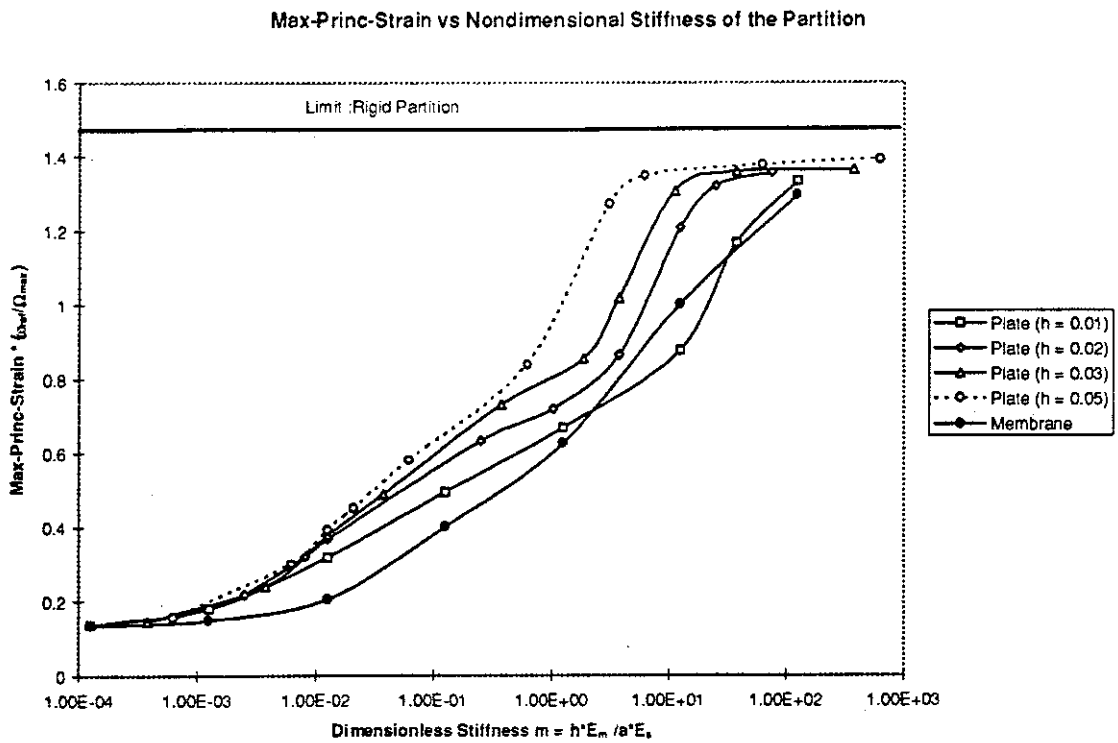

Figure 4.3.9: Peak value of the Max. Principal Strain vs partition membrane stiffness

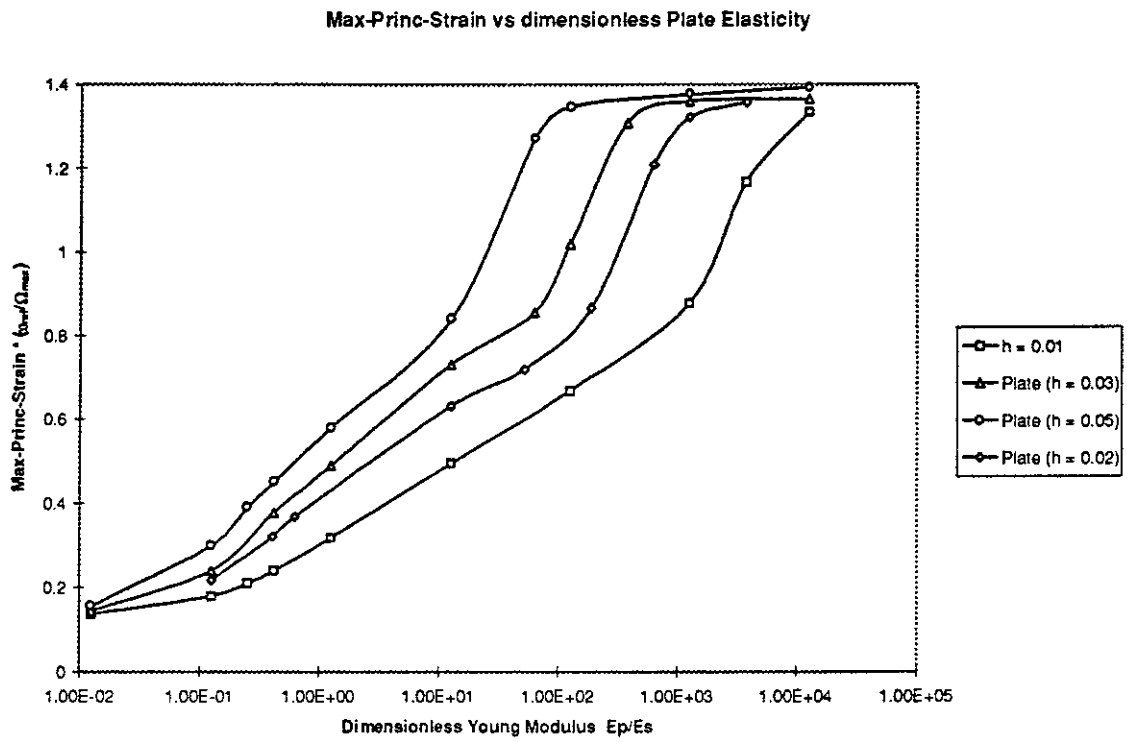

Figure 4.3.10: The effect of changing partition stiffness by increasing Young's modulus of elasticity for fixed values of partition stiffness.

5.0 Conclusions

Benchmark solutions have been developed for a 2D plane strain model for shear strain predictions that can be solved for elastic and viscoelastic cerebral material models. These solutions have been compared with numerical(FE) predictions and the limitations of the numerical models have been identified. The numerical solutions showing an early arrival of response compared with the analytical result. The actual values of the Principal Strain are in reasonable agreement between the two approaches. The numerical results also show that the response of the 2D model is linear with the magnitude of the applied rotational velocity to the periphery when the maximum velocity is lower than the angular shear wave velocity.

For relaxation effects there is increased peak strain compared to the elastic case, when the relaxation frequency is greater than approximately ten times the reference frequency ω_{ref} ($=\frac{c}{a}$). This is a significant effect and the strain is more sensitive to lower frequency contributions, i.e. longer duration input. The introduction of a rigid partition (modelling a Falx) produces a model with both shear and compressive strain effects. The maximum strain occurs close to the tip of the partition and is relatively insensitive to reasonable variation in the material properties of the cerebral matter or the non-viscous fluid surrounding the partition. The gap, with no fluid included, produces a maximum response in the elastic models for a zero gap and for viscoelastic material the effect is similar but with much greater sensitivity to variation of the gap size. The inclusion of non viscous fluid in the gap reduces the strains as would be expected.

The partition depth, how it is fixed to the skull and its stiffness properties alter the strain response. The maximum strain response is not obtained for the longest partition although more rigidly attaching the partition to the skull, that has the imposed rotation applied to it, does cause the strains to increase. One would expect this latter result to be produced as more load is applied to the cerebral matter if the partition does not rotate at its base. By introducing either membrane stiffness or bending stiffness of the partition it appears that the strain in the cerebral material is higher due to the bending compared to the membrane property of the partition. In both cases increasing the stiffnesses causes the strain to approach that obtained for the rigid partition, as anticipated.

Further work can now be directed into producing realistic 3 D models of the skull and brain and applying loads, simulating typical impacts. The viscoelastic models have shown some need for improvement, possibly by reformulating, and there is still no suitable viscous fluid model available that may be needed for the CSF. Measurements of the cerebral and Falx material properties are still limited, although this study has assisted in quantifying the frequency range for which the properties are required.

REFERENCES:

Baker, W.E., Westine, P.S. and Dodge, F.T. 1973. Similarity methods in engineering dynamics: theory and practice of scale modelling, Hayden Book Co., Inc., Rochelle Park, N.J.

Bandak F.A. and Eppinger, R.H. 1994: A 3D Finite Element Analysis of the Human Brain Under Combined Rotational and Translational Accelerations. 38th Stapp Car Crash Conf. SAE paper 942215, 1994, pp. 145-163.

Cheng, L. Y., Rifai S. Khatua T. and Piziali R. L. (1990). Finite element analysis of diffuse axonal injury. Proc. of the 34th Stapp Car Crash Conf., SAE Paper 900547, pp. 141-154.

Chu, C. S. and Lee, M. C. (1991): Finite element analysis of cerebral contusion. Advances in Bioengineering, ASME-BED-Vol. 20, pp. 601-604.

DiMasi, F., and Eppinger R. H. , Gabler III H. C. and Marcus J. H. (1991a): Simulated head impacts with upper interior structures using rigid and anatomic brain models. Auto & Traffic Safety. Summer, pp. 20-31.

DiMasi, F., Marcus J. H. and Eppinger R. H. , (1991b): 3D anatomic brain model for relating cortical strains to automobile crash loading. Proc. 13th Int. Techn. Conf. on Experimental Safety Vehicles, paper No. 91-S8-O-11.

Fallenstein G. T., Hulce V.D., and Melvin, J.W. (1969): Dynamic mechanical properties of human brain tissue. J. Biomechanics, vol. 2, pp 217-226, 1969.

Firoozbakhsh, K. K. and DeSilva, C. N. (1975): A Model of Brain Shear Under Impulsive Torsional Loads. Journal of Biomechanics. Vol. 8. pp. 65-73.

Galbraith, C. G. and Tong, P. (1988): Boundary conditions in head injury finite element modeling. 16th Annual Int. Workshop on Human Subjects for Biomechanical Research. pp. 179-193.

Galbraith, J.A., Thibault L.E. and Matteson D.R. (1993): Mechanical and electrical responses of squid giant axon to simple elongation. J. Biomech. Eng. 115, pp. 13-22.

Galford J. E. and McElhaney J. H. (1970): A viscoelastic study of scalp, brain and dura. J. Biomechanics, vol. 3, pp 211-221,1970.

Gennarelli T. A., Ommaya A. K. and Thibault L. E. (1972): Comparison of translational and rotational head motions in experimental cerebral concussion. Proc. of 15th Stapp Car Crash Conf. pp. 797-803.

Gradshteyn I.S. and Ryzhik I.M. Table of integrals, series and products. 4th edition, Academic Press, London, 1983.

Hardy, W.N., Khalil T.B. and King, A.I., (1994). Literature review of head injury biomechanics. Int. J. Impact Eng. vol. 15, pp. 561-586.

Hickling, R. and Wenner, M. L. (1973): Mathematical model of head subjected to an axisymmetric impact. J. Biomechanics, 6, p.115-132.

Hirakawa K., Hashizume K. and Hayashi T.(1981) : Viscoelastic Properties of Human Brain Tissue: -For the Analysis of impact Injury (for impact injury modelling). 33; pp. 1057-1065, 1981.

Holbourn, AHS. (1943): Mechanics of Head injuries. Lancet 2, pp. 438-441.

Kreyszig E.: Advanced Engineering Mathematics, 7th edition, Wiley, New York, 1992.

Kumaresan S. and Radhakrishnan S. (1995): Importance of partitioning membranes of the brain and the influence of the neck in head injury modelling.
Lee M-C., Melvin J. W. and Ueno K. (1987): Finite element analysis of traumatic subdural haematoma. Proceed. 31st Stapp Car Crash Conf. pp. 202-212.
Lee, Y-C. and Advani S.H. (1970): Transient response of a sphere to torsional loading- A Head Injury Model. Mathematical Biosciences, vol. 6, pp 473-486.
Liu, Y. K., Chandran, K. B. and Rosengerg, D. U. (1975): Angular Acceleration of a Viscoelastic (Kelvin) Material in a Rigid Spherical Shell - A Rotational Head Injury Model. Journal of Biomechanics. Vol. 8. pp. 285-292.
Ljung C. 1975: A Model for Brain Deformation Due to Rotation of The Skull. J. Biomechanics, vol. 8, pp. 263-274.
Ljung C. (1980): On scaling in head injury research. IRCOBI, pp. 209-217.
McElhaney J.H., Roberts V.L. and Hilyard J.F. 1976: Handbook of Human Tolerance. Japan Automotive Research Institute, Inc. Japan, 1976.
Margulies, S.S. and Thibault, L.E. An analytical model of traumatic diffuse brain injury. ASME, J. Biomech. Eng., vol. 111, 1989, pp. 241-249.
Margulies, S.S., Thibault L.E. and Gennarelli T. A.(1990): Physical model simulation of brain injury in the primate. Journal of biomechanics, vol. 23 (8), pp 823-836.
Ruan, J.S., Khalil, T. and King A.I. 1991: Human head dynamic response to side impact by finite element modelling. J. Biomech. Engineering, vol. 113, pp. 276-282, 1991.
Shuck LZ., and Advani SH. (1972): Rheological response of human brain tissue in shear. J. Basic Eng. p. 905-911, 1972.
Skudrzyk E. 1971: The Foundations of Acoustics: Basic mathematics and Basic Acoustics. Springer-verlag, Vienna, 1971.
Stephenson, G. An Introduction to Parietal Differential Equations for Science Students. 2nd edition, Longman, London, 1974.
Thibault KL. and Margulies SS.(1996): Material properties of the developing porcine brain. Proc. IRCOBI, p. 75-85, 1996.
Tong P., DiMasi F., Carr, Eppinger R. H., Marcus J. H. and Galbraith, C. G. (1989): Finite element modelling of head injury caused by inertial loading. Proc. 12th int. Conf. on Experimental Safety Vehicles, pp. 617-626.
Trosseille X., Tarriere C., Lavaste F., Guillon F., Domont A. (1992): Development of a FEM of the human head according to a specific test protocol. Proc. of the 36th Stapp Car Crash Conf., pp. 235-253.
Turquier F., Trosseille X., Tarriere C., Lavaste F., Domont A., Kang H. S. and Willinger R. (1996): Validation study of a 3D finite element head model against experimental data, Proc. of the 40th Stapp Car Crash Conf., pp. 283-294, 1996.
Ueno, K. and Melvin, J.W. 1995: FE model study of head impact based on hybrid III head acceleration: The effects of rotational and translational acceleration. J. of Biomech. Eng., vol. 117, pp. 319-328.
Willinger, R. Taleb, L. Viguier P. and Kopp C-M., 1994: Rotation-Translation Duality in Head Trauma: Perceptive and Objective Evidence. Proceed. IRCOBI, pp. 63-76.